Identification of hub necroptosis-related lncRNAs for prognosis prediction of esophageal carcinoma

Zhengdong Luo[1,*], E Ding[1,*], Longchen Yu[1], Wenwu Wang[2], Qining Guo[1], Xinyang Li[1], Yifeng Wang[1], Tingting Li[1], Yi Zhang[1,*], Xin Zhang[1,*]

[1]Department of Clinical Laboratory, Qilu Hospital of Shandong University, Jinan, Shandong Province, China
[2]Hangzhou Lin'an District Fourth People's Hospital, Hangzhou, Zhejiang Province, China
*Equal contribution

Correspondence to: Yi Zhang, Xin Zhang; **email:** yizhang@sdu.edu.cn, xinzhang@sdu.edu.cn

ABSTRACT

Necroptosis is a newly identified programmed cell death associated with the biological process of various cancers, including esophageal carcinoma (ESCA). Meanwhile, the dysregulation of long non-coding RNAs (lncRNAs) is greatly implicated in ESCA progression and necroptosis regulation. However, the lncRNAs involved in regulating necroptosis in ESCA are still unclear. In this study, we aim to explore the expression profile of necroptosis-related lncRNAs (NRLs), and evaluate their roles in ESCA prognosis and treatment. In the present study, 198 differentially expressed NRLs were identified between the ESCA and adjacent normal tissues through screening the data extracted from the Cancer Genome Atlas (TCGA) database. And, a prognostic panel consisting of 6 NRLs was constructed using the LASSO algorithm and multivariate Cox regression analysis. The ESCA patients with high risks had a markedly reduced survival time and higher mortality prevalence. Moreover, C-index of 6 NRLs-panel was superior to 48 published prognostic models based on lncRNAs or mRNAs for ESCA. There were significant differences between the high-risk and low-risk groups in tumor-related pathways, genetic mutations, and drug sensitivity responses. *In vitro* analysis revealed that inhibition of PVT1 impeded the proliferation, migration, and colony formation of ESCA cells, increased the expressions of p-RIP1 and p-MLKL and promoted necroptosis. By contrast, PVT1 overexpression resulted in a decrease in necroptotic cell death events, thus promoting tumor progression. Collectively, the established 6-NRLs panel was a promising biomarker for the prognostic prediction of ESCA. Moreover, our current findings provided potential targets for individualized therapy for ESCA patients.

INTRODUCTION

As one of the most common gastrointestinal tumors worldwide, esophageal carcinoma (ESCA) is often associated with delayed diagnosis and inferior outcomes [1, 2]. At present, surgery remains the only curative measure for treating early ESCA, while it has little clinical success for patients with advanced cancer [3]. Despite the effective improvement in early detection and combination therapy regimens, the 5-year survival rate of ESCA patients is still as low as 20% [4, 5].

Although some combined therapeutic regimens have ameliorated the survival time of patients with advanced diseases [6, 7], they are still controversial in clinical responses. The effective prediction of the prognosis is important for appropriate treatment planning. Therefore, it is urgently necessary to identify novel biomarkers to predict the prognosis of ESCA.

As a newly identified programmed cell death, necroptosis is regulated by TNF-α and RIPK1/RIPK3-dependent phosphorylation of MLKL [8, 9], and such

a process is different from apoptosis, necrosis, pyroptosis, ferroptosis, and so on [10]. Accumulating evidence has shown that necroptosis is widely associated with tumorigenesis and the progression of malignancies [11, 12]. It has been reported that immunogenic necroptotic cells can be adopted as vaccines to induce efficient antitumor immunity to eliminate tumor cells [13]. Furthermore, Zheng et al. [14] have revealed that STAT3β is up-regulated in the cytoplasm of esophageal squamous cell carcinoma (ESCC), leading to enhanced sensitivity to concurrent chemoradiotherapy (CCRT) via inducing necroptosis. Importantly, studies have found that necroptosis is closely related to tumor-infiltrating lymphocytes, which can be adopted as an independent prognostic parameter of ESCC [15]. Collectively, necroptosis-related regulators may be potential prognostic biomarkers for ESCA.

Long non-coding RNAs (lncRNAs) are a group of special non-coding RNAs with transcript lengths over 200 nucleotides [16], which are generally involved in the regulation of protein-encoding genes through epigenetic modulations, transcriptional regulation, and post-transcriptional regulation [17, 18]. Increasing studies have implicated that lncRNAs contribute to the development of ESCA [19]. Studies have found that LINC00680, a competing endogenous RNA (CeRNA), can sponge microRNA-423-5p to induce the expression of PAK6 and promote the progression of ESCC [20]. Furthermore, lncRNAs VESTAR and CASC9 are overexpressed in ESCC and promote cancer metastasis through other mechanisms, including transcriptional regulation and epigenetic modification [21, 22]. At present, many reports have revealed that the necroptosis-related lncRNAs (NRLs) may be used as prognostic biomarkers for some cancers [23–25]. However, their potential prognostic value in ESCA remains largely unexplored.

LncRNA plasmacytoma variant translocation 1(PVT1) is located on chromosome 8 of the c-Myc gene and is abnormally expressed in multiple malignancies, including nasopharyngeal carcinoma [26], colorectal cancer [27], ovarian cancer [28], and so on. PVT1 usually interacts with c-Myc to mediate malignant tumor progression, such as proliferation, invasion, metastasis, therapeutic resistance, etc. In general, PVT1 overexpression is often associated with poor prognosis in patients, and it has been regarded as a novel carcinogenic factor [29]. Studies discovered that PVT1 is highly expressed in renal clear cell carcinoma tissues and with poor prognosis in patients. Functional experiments demonstrated that PVT1 could stabilize the expression of HIF2α by regulating the ubiquitination-dependent degradation pathway,

thereby promoting the invasion and metastasis of cancer cells [30]. Furthermore, PVT1 can act as a sponge to competitively bind miR-128-3p and elevate FOXQ1, inducing epithelial-mesenchymal transformation of cancer cells [31]. In addition, HAT1 promoted the expression of PVT1 by promoting the binding of BRD4 to the PVT1 promoter, thereby mediating gemcitabine resistance [32]. Intriguingly, PVT1 may also serve as a good prognostic indicator for the early stages of some cancers, such as ovarian carcinoma [33]. Nevertheless, the detailed mechanism by which PVT1 regulated esophageal carcinoma progression remains poorly understood and thus needs to be further elucidated.

In the present work, we thoroughly explored the expression pattern of NRLs in ESCA and established a prognostic panel based on six NRLs by least absolute shrinkage and selection operator (LASSO) and multi-Cox regression. Moreover, we assessed its predictive value using principal component analysis (PCA), time-dependent receiver operating characteristic (ROC), concordance index (C-index), nomogram, tumor mutational burden (TMB) analysis, and chemotherapy response analysis of ESCA patients. Besides, we further performed the gene set enrichment analysis (GSEA) to explore its underlying mechanisms. Finally, the expression of one NRL, PVT1, in ESCA cells was detected, suggesting its role in necroptosis. Collectively, these data provided valuable insights into the progression and prognosis of ESCA.

MATERIALS AND METHODS

Information acquirement and data manipulation

A total of 162 ESCA tissue samples and 11 adjacent non-tumor tissue samples were acquired from The Cancer Genome Atlas (TCGA, https://portal.gdc.cancer.gov/), and their corresponding transcriptomic FPKM data, somatic mutations, and clinical information were also collected. Patients with missing information on survival time or those with survival time < 1 month were excluded from the analysis. In addition, 159 necroptosis-related genes (NRGs) were acquired from the Kyoto Encyclopedia of Genes and Genomes (KEGG, https://www.kegg.jp/) (Supplementary Table 1).

Enrichment and interaction analysis of differentially expressed NRGs (DE-NRGs)

The DE-NRGs between ESCA and adjacent normal tissues were identified using the "limma" package. Subsequently, Metascape (https://metascape.org/gp/index.html#/) was adopted to conduct the functional enrichment analysis and protein-protein

interaction (PPI) network of DE-NRGs. Besides, NRG mutations were alsoassessed in ESCA using the cBioPortal website (http://www.cbioportal.org/).

Identification of prognostic differentially expressed NRLs (DE-NRLs)

To identify the lncRNA co-expressed with NRGs in ESCA, we obtained lncRNA expression matrix from the TCGA. Then, necroptosis-related lncRNAs (NRLs) were identified using Pearson correlation analysis (|coefficient | >0.4 and p < 0.001, Wilcoxon test) based on their expression. Subsequently, DE-NRLs were screened using the "limma" package.

Construction of the NRLs-associated prognostic panel and nomogram

The optimal panel of prognostic NRLs was determined using the LASSO-Cox algorithm, and a corresponding prognostic panel was constructed. In the meantime, we equally divided all patients into training and testing groups, the risk score of each patient with ESCA was calculated using the formula as follows:

$$Risk\ Score = \sum_{i=1}^{n} Coef(i) \times x(i)$$

Coef (i) represents the coefficient, and x(i) represents the standardized level of each NRL. According to the median risk score of each patient, all patients were categorized into low-risk and high-risk groups. Subsequently, the predictive capacity of the 6-NRLs prognostic panel was assessed for various clinicopathological characteristics by the log-rank method. Besides, a nomogram was generated, and the 1-, 3- and 5-year recurrence rates of ESCA patients were predicted based on such a nomogram.

Models comparison

We retrieved the published prognostic signatures of ESCA constructed based on lncRNAs or mRNAs since 2017 using multiple databases. Then, "timeROC" and "survcomp" packages were applied for model comparison to evaluate the predictive ability of each model.

Pathway enrichment analysis and TMB

The potential enrichment pathways among different risk groups were identified using the GSEA with the "clusterProfiler" package. Moreover, "maftools", "survival," and "survminer" were applied to reveal the difference and survival of the TMB between the above-mentioned two groups of patients.

Identification of potential compounds in the treatment response of ESCA

The "pRRophetic", "ggpub", and "ggplot2" packages were used to identify the potential chemotherapeutic drugs that might be applied for ESCA therapy. Moreover, the Wilcoxon signed-rank test was adopted to determine the half-maximal inhibitory concentration (IC50) of common compounds between high-risk and low-risk groups.

Cell culture and reagents

The human esophageal epithelial cells (HEECs) and human esophageal cell lines, including ECA109, KYSE150, and KYSE510, were maintained in RPMI-1640 medium (Gibco, Thermo Fisher Scientific, USA) supplemented with 10% fetal bovine serum (Gibco, Thermo Fisher Scientific, USA) and penicillin-streptomycin cocktail (1:100; Solarbio, Beijing, China) at 37° C in a humidified atmosphere containing 5% CO_2. TSZ (TNF-alpha, Smac, and z-VAD) (Selleck, Houston, TX, USA) and necrostatin-1 (MedChemExpress, Monmouth Junction, NJ, USA) were used as previously described [34].

RNA extraction and RT-qPCR

Total RNA was isolated from the cells using TRIzol Reagent (Invitrogen, Eugene, OR, USA). Subsequently, purified RNA was reversely transcribed to cDNA using HiScript III RT SuperMix (Vazyme, Nanjing, China). RT-qPCR was performed using ChamQ Universal SYBR qPCR Master Mix (Vazyme, Nanjing, China). The PVT1 plasmid was adopted as a positive control, while the negative control contained all components except for cDNA. Each experiment was carried out three times. GAPDH was employed as the housekeeping gene. The relative expression of PVT1 was determined using the $2^{-\Delta\Delta Ct}$ method. Supplementary Table 3 lists the primer sequences.

Vector construction and transfections

For PVT1 overexpression, the full-length sequence of PVT1 was synthesized and cloned into the pcDNA3.1(+) vector (Hanbio Biotechnology, Shanghai, China). The shRNAs targeting PVT1 were synthesized by Sangon Biotech Co., Ltd. (Shanghai, China), and Supplementary Table 3 lists the corresponding sequences. Afterward, the transfection assays were carried out using Lipofectamine™ 3000 according to the manufacturer's instructions (Invitrogen, Thermo Fisher Scientific, USA).

Migration assay

To conduct migration assays, uncoated transwell inserts with 8 μm pores were inserted into 24-well plates. Next, we added 700 μl of RPMI-1640 medium with 20% FBS to each lower chamber, and a total of 5×104 infected ECA-109, KYSE-150, or KYSE-510 cells were resuspended in 200 μl serum-free medium in each upper chamber. The remaining cells in the upper chamber were wiped clean with a cotton swab after 24 hours of incubation (48 hours for KYSE-510 cells) at 37° C, 5%CO2. The bottom membrane with invaded cells was fixed with 4% paraformaldehyde and dyed with 0.1% crystal violet (Solarbio, Beijing, China) for 30 min, respectively. The migrated cells were counted in five random fields at 200× magnification using ImageJ software. The results were expressed as the mean number of migrated cells per field.

Colony formation assay

For colony formation assay, 1000 infected ECA-109, KYSE-150, or KYSE-510 cells were inoculated into the six-well plates and incubated for 12 days at 37° C, 5% CO2. When clones were visible to the naked eye, the cells were washed with phosphate-buffered saline (PBS) twice and fixed with 4% paraformaldehyde for 20 min. When clonal colonies were visible ($\geq$ 50 cells/colony), the cells were washed twice with phosphate-buffered saline (PBS) and fixed with 4% paraformaldehyde for 20 minutes, followed by staining with 0.1% crystal violet solution for 30 min. After being air-dried, the colonies were photographed and counted.

Cell counting kit-8 assay

To evaluate the proliferative capacity of infected cells, a cell counting kit-8 (CCK-8) experiment was conducted. Specifically, infected ECA-109, KYSE-150, or KYSE-510 cells were inoculated into 96-well plates at a density of 3000 cells per well for proliferation for 0, 1, 2, 3, 4, and 5 days, then 10ul CCK-8 reagent (Solarbio, Beijing, China) was added to each well and incubated for 2 h at 37° C. for 2 hours. The absorbance at 450 nm was measured using a microplate reader (Thermo Fisher Scientific, USA).

Western blotting analysis

Briefly, ESCA cells under different treatments were rinsed with cold PBS two times and then lysed using RIPA buffer (Thermo Fisher Scientific, USA) containing protease inhibitors (Solarbio, Beijing, China) and phosphatase inhibitors (Solarbio, Beijing, China). Moreover, the contents of soluble proteins were determined by the BCA protein detection kit (Thermo

Fisher Scientific, USA). Subsequently, Western blotting analysis was carried out as previously described [34] using antibodies against RIP (#3493), phospho-RIP (Ser166) (#65746), MLKL (#14993), phospho-MLKL (Ser358) (#91689), and GAPDH (#8884) (1:1,000; Cell Signaling Technology, Danvers, MA, USA).

Data availability

The data supporting the conclusions of this study could be acquired from TCGA database (https://portal.gdc.cancer.gov/) and KEGG website (https://www.kegg.jp/). Other details are available from the corresponding author upon a reasonable request.

RESULTS

Differentially expressed NRGs

Figure 1 illustrates the flowchart for the current work. Supplementary Table 2 shows the clinical details of ESCA patients. We identified 27 DE-NRGs between the tumor and adjacent normal tissues (|fold change| > 1.5 and FDR < 0.05) (Supplementary Figure 1A and Supplementary Table 4). Moreover, we performed enrichment analyses of the DE-NRGs using the Metascape database. Unsurprisingly, these NRGs primarily participated in necroptosis, influenza A, measles virus infection, TNF-α signaling pathway, and so on (Supplementary Figure 1B), and a PPI network of DE-NRGs was established (Supplementary Figure 1C and Supplementary Table 7). Lastly, we found that the genetic alteration of seven NRGs exhibited a mutation rate of $\geq$3% using cBioPortal, among which FADD had the highest mutation rate (14%) (Supplementary Figure 1D).

Construction of an NRLs-based prognostic signature in ESCA

We identified 1,221 NRLs with a co-expression correlation in ESCA (Supplementary Table 5). Among them, 198 DE-NRLs were identified between the ESCA and adjacent normal tissues, including 20 up-regulated and 178 down-regulated NRLs (|fold change| > 2 and FDR < 0.05) (Figure 2A). Subsequently, the prognostic significance of NRLs was shown by the univariate Cox regression and heatmap (Figure 2B, 2C). Subsequently, a prognostic panel consisting of 6 NRLs was constructed using the LASSO algorithm and multivariate Cox regression analysis (Figure 2D, 2E). The risk score = (7.7678) × AC027612.2 + (0.6060) × IDH2-DT + (0.5578) × PVT1 + (0.7428) × LINC02608 + (-1.0974) × AC021016.2 + (1.6266) × AC084262.1). The ESCA patients were grouped based on their median risk scores. Figure 3 exhibits the status

of survival, the distribution of risk scores, and the overall survival (OS) of six NRLs in the training, testing, and entire cohort. The ESCA patients with lower risk scores exhibited a reduced risk of death and longer survival time (Figure 3G–3I). Importantly, compared with AGs, NRGs, and NRLs, PCA indicated that the 6-risk NRLs had optimal discrimination capacity, which could better distinguish high- and low-risk groups (Supplementary Figure 2).

Assessment of clinicopathological indicators of the NRLs panel

A forest plot was established to further determine independent prognostic indicators for ESCA patients based on univariate and multivariate Cox analyses (Figure 4A, 4B). Our results revealed that grade was an independent factor influencing the prognosis of ESCA. Next, the 1-, 3- and 5-year overall recurrence rates in ESCA patients were predicted using a nomogram containing clinicopathological features (Figure 4C). In addition, our data indicated that the area under ROC curves (AUCs) of 1-year in the entire cohort was 0.784 (Figure 4D), which performed better than other clinicopathological features in the prognostic prediction of ESCA patients. Besides, the 3- and 5-year AUC for the entire cohort were 0.827 and 0.764, respectively (Figure 3G). Moreover, the AUCs of both training and testing sets also displayed good predictive performance. In the training cohort, the AUCs of 1-, 3-, and 5-year
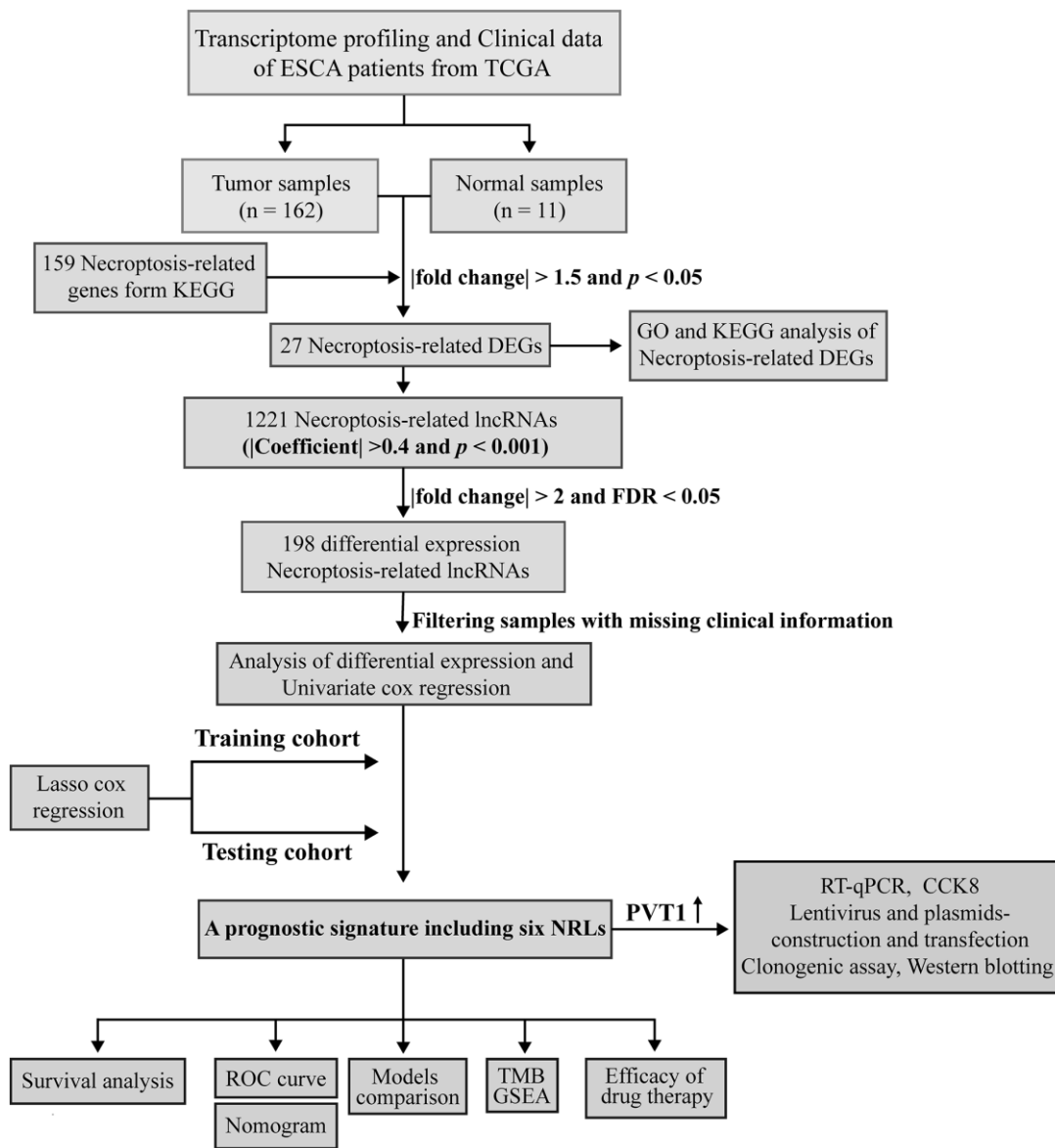

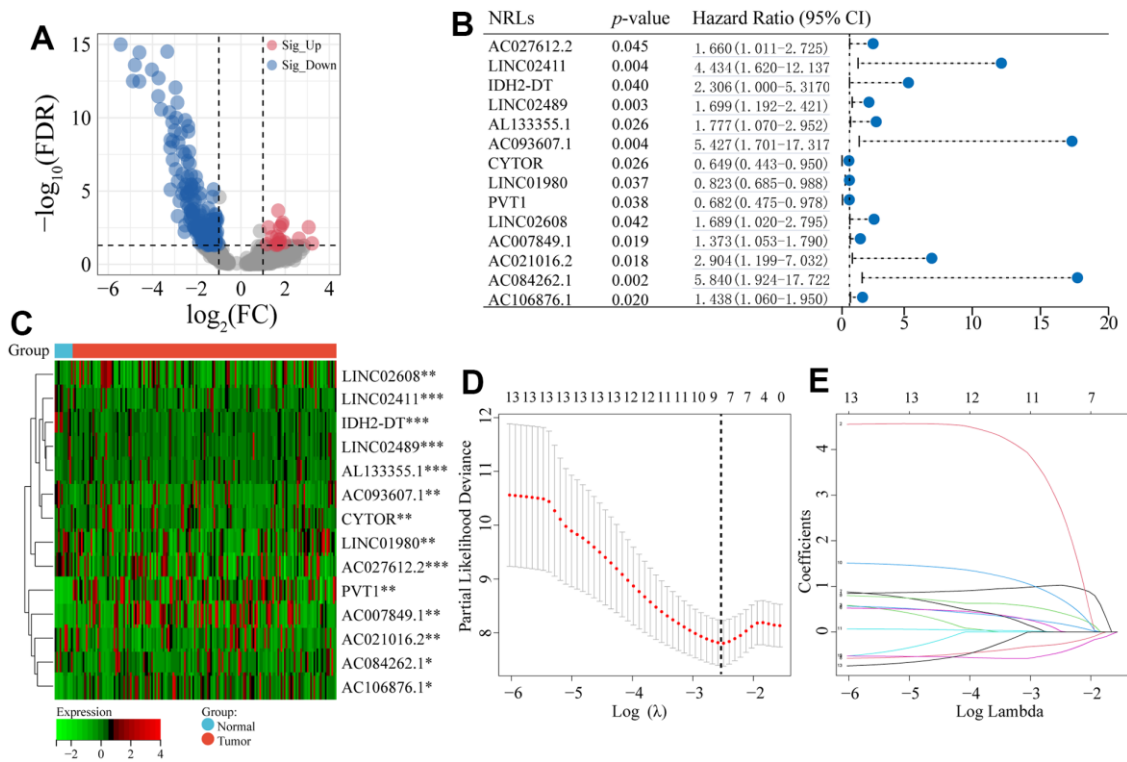**Figure 1. Workflow based on a comprehensive analysis of NRLs.**

Figure 2. Differentially co-expressed NRLs and LASSO regression. (**A**) The volcano plot of the significant differential expression of NRLs. (**B**, **C**) A forest plot and a heatmap of the 14 prognostic NRLs. (**D**) Ten-fold cross-validation for error rate. (**E**) Least absolute shrinkage and selection operator regression. Asterisks (*) stand for significance levels, ** p < 0.01, * p < 0.05.
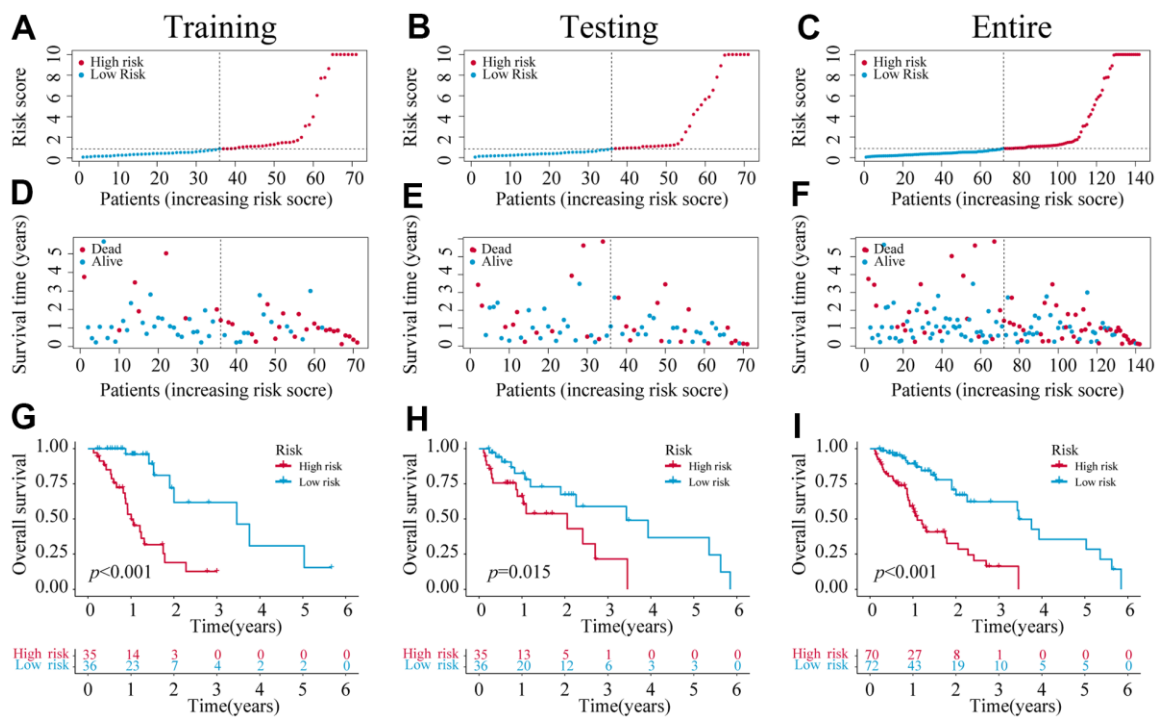

Figure 3. The construction of a 6-NRLs prognostic signature. (**A–C**) The risk score of six prognostic NRLs. (**D–F**) Survival status distribution of six prognostic NRLs. (**G–I**) Kaplan–Meier survival curves of high-risk and low-risk patients in training, testing, and entire groups.

survival were 0.853, 0.905, and 0.804, respectively (Figure 4E). In the testing cohort, the AUCs of 1-, 3- and 5-year survival were 0.703, 0.737, and 0.724, respectively (Figure 4F). Finally, the calibration curves displayed good consistency between the actual and predicted survival possibility at 1-, 3-, and 5 years (Figure 4D–4J). Subsequently, we assigned ESCA patients into high- and low-risk groups based on age, gender, grade, stage, T, and N. For each clinicopathological variable, the patients with high risks had a markedly reduced survival time and higher mortality prevalence compared with the low-risk group (Supplementary Figure 3).

Evaluation of the NRLs signature

A total of 48 prognostic signatures for ESCA based on lncRNA or mRNA were included in the comparison (Supplementary Table 6). The results showed that the 1- and 3-year AUC of the six-NRLs panel for the entire cohort were higher than those of other prognostic models, respectively (Figure 5A, 5B), and 5-year AUC was higher than those of most prognostic models (Figure 5C). Furthermore, we assessed NRLs discrimination by C-index. Our data displayed that the C-index [95% confidence interval] of six NRLs was 0.759 [0.721, 0.797], which was superior to other prognostic models (Figure 5D).

Pathway enrichment analysis

To elucidate the underlying molecular mechanism of the 6-NRLs prognostic panel in ESCA, we investigated critical pathways between the two groups via GSEA. We found that the citrate and TCA cycle, mTOR signaling pathway, and oxidative phosphorylation were remarkably enriched in the high-risk group (Supplementary Figure 4A), while the notch signaling pathway, antigen processing and presentation, pentose phosphate pathway, and TGF-β and hedgehog signaling pathway were enriched in the low-risk group (Supplementary Figure 4B).

TMB analysis

Accumulating evidence has revealed that TMB has become a promising biomarker for the immune response to malignancies [35, 36]. To assess the correlation between different risk groups and TMB, we calculated TMB scores of high and low-risk groups (the top 15 genes with the highest mutation) according to TGCA somatic mutation data. We found that the high-risk group had a higher mutation frequency for most genes than the low-risk group, except for MUC16, DNAH5, HMCN1, ZNF804B, and CSMD1 (Figure 6A, 6B). However, as a whole, no significant difference in TMB was found

between these two groups (Figure 6C). Next, the ESCA patients were assigned into high- and low-mutation groups based on the TMB scores. We found that the high-mutation group had a reduced survival possibility compared with the low-mutation group (Figure 6D). Interestingly, we confirmed that the 6-NRLs panel performed better than TMB in the prognostic prediction and found that integrating two signatures might be a more appropriate clinical strategy (Figure 6E).

Identification of potential compounds for therapeutic response to ESCA

Eight therapeutic compounds exhibited marked differences in drug sensitivity between high- and low-risk groups, indicating that the IC50 values of four drugs, EHT.1864 (RAC family inhibitor), Nutlin.3a (Rebemadlin), BIRB.0796 (Doramapimod), and PD.0332991 (Palbociclib), in the low-risk group, were higher compared with the high-risk group (Figure 6F), while the other four drugs, BIBW2992 (Afatinib), LFM.A13 (BTK inhibitor), WO2009093972 (PI3K inhibitor), and Bosutinib, had higher sensitivity compared with the low-risk group (Figure 6G). These findings contributed to exploring better personalized therapeutical strategies.

Effects of PVT1 on the proliferation, migration, and necroptosis of ESCA cells

Consistent with the above results, only the expression of PVT1 was increased in ESCA tissues among the six prognostic NRLs compared with normal tissues (Figure 7A). High expression of PVT1 was positively correlated with the poor outcomes of ESCA patients (Figure 7B). To explore the potential roles of PVT1 in the progression of ESCA, we first assessed the expression pattern of PVT1 in normal HEECs and available ESCA cell lines (ECA-109, KYSE-150, and KYSE-510). Compared with HEEC cells, ECA-109 and KYSE-150 showed high expression of PVT1, while KYSE-510 exhibited low expression of PVT1 (Figure 7C). Accordingly, ECA-109 and KYSE-150 were selected for deletion of PVT1, KYSE-510 was chosen for overexpression of PVT1, and the transfection efficiencies were estimated by RT-qPCR (Figure 7D, 7E and Supplementary Figure 5A). *In vitro* experiments revealed that depletion of PVT1 significantly inhibited the proliferation and migration of ECA-109 and KYSE-150 cells compared with the controls (Figure 7F, 7G and Supplementary Figure 5B, 5C), while overexpression of PVT1 in KYSE-510 displayed the opposite results (Figure 7H, 7I). To further confirm whether PVT1 was an essential regulator for necroptosis, we observed the necroptosis of ESCA cells treated with TSZ (1:1,000) and Nec-1 (50 μm/mL).
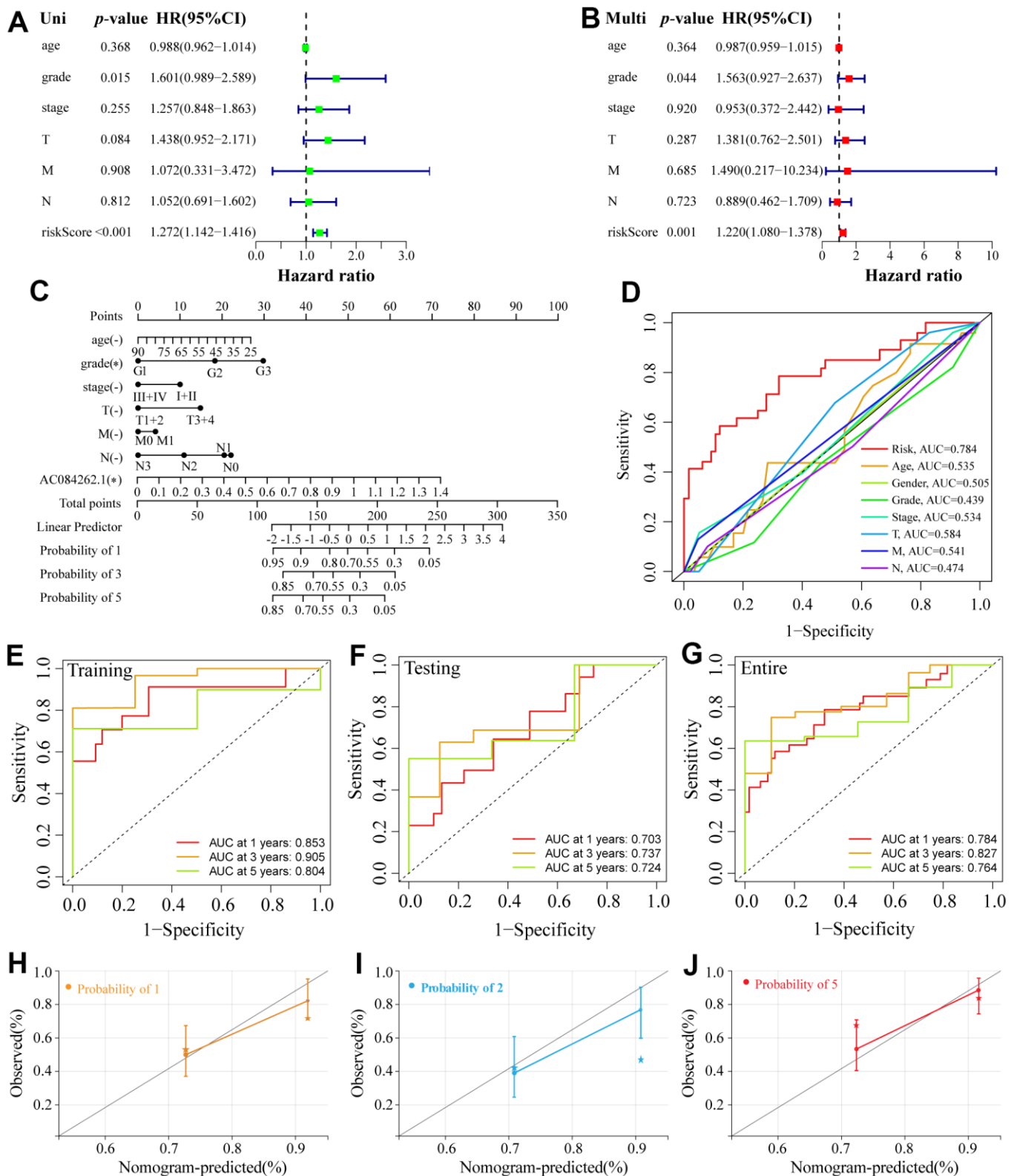
Figure 4. Establishment of a nomogram and ROC analysis. (**A**, **B**) The forest plot of the univariate and multivariate Cox regression. (**C**) A nomogram combining clinicopathological variables and risk score predicts 1-, 3-, and 5-year OS of ESCA patients. (**D**) The ROCs curve for different clinicopathological variables. (**E–G**) The ROCs curve for 1-, 3-, and 5-year survival time training, testing, and entire groups are based on the risk score. (**H–J**) Calibration curve of the nomogram to predict the probability of the 1-, 3-, and 5-year OS.

Figure 8A reveals that compared with the control group, more ECA-109 PVT1-sh cells underwent necroptosis, and this phenotype was strengthened upon TSZ treatment, while Nec-1 alleviated such necroptotic death. Likewise, the Western blotting analysis exhibited that depletion of PVT1 increased the expressions of p-RIP1 and p-MLKL at the protein level (Figure 8B), and similar results were confirmed in KYSE-150 PVT1-sh cells (Supplementary Figure 5D, 5E). In contrast, overexpression of PVT1 inhibited necroptotic cell death, while TSZ significantly promoted necroptotic phenotype in ECA-109 PVT1-sh cells (Figure 8C), and overexpression of PVT1 reduced the expressions of p-RIP1 and p-MLKL at the protein level (Figure 8D). Taken together, these findings indicated the underlying role of PVT1 in the necroptosis of ESCA cells.

DISCUSSION

This work put forward several new revelations. First, a 6-NRLs signature was constructed and internally validated for predicting the prognosis of ESCA. Second, we discovered the good accuracy and stability of 6-NRLs panel using multi-models comparison. Third, we have confirmed that lncRNA PVT1 can inhibit necroptosis, thus promoting the progression of ESCA.

As a regulated form of necrosis, necroptosis can result in organelle swelling, cell membrane rupture, and decomposition of cytoplasm and nucleus [37]. Accumulating evidence reveals that necroptosis participates in the pathogenesis of various malignancies and plays a fundamental role in the prognosis and treatment response of patients [38]. Therefore, targeting necroptosis has emerged as a potential antitumor strategy [39]. Recently, some lncRNA-based signatures related to necroptosis have been used to evaluate the outcomes of patients with various tumors, including lung adenocarcinoma [23], colon cancer [25], and stomach cancer [24]. However, the prognostic value of NRLs in ESCA has not been well documented.

In the present study, a total of 27 differentially expressed NRGs was identified, many of these DE-NRGs may contribute to activating necroptosis, such as IL33, GLUL, and RIPK1. Interestingly, we observed that compared with normal tissues, these genes were down-regulated in ESCA tissues, suggesting that necroptosis inhibition may be a driving factor mediating the development of ESCA. Next, we chose 14 prognosis-related NRLs from 198 DE-NRLs, and then a prognostic model was constructed using six NRLs (AC027612.2, IDH2-DT, PVT1, LINC02608, AC021016.2, and
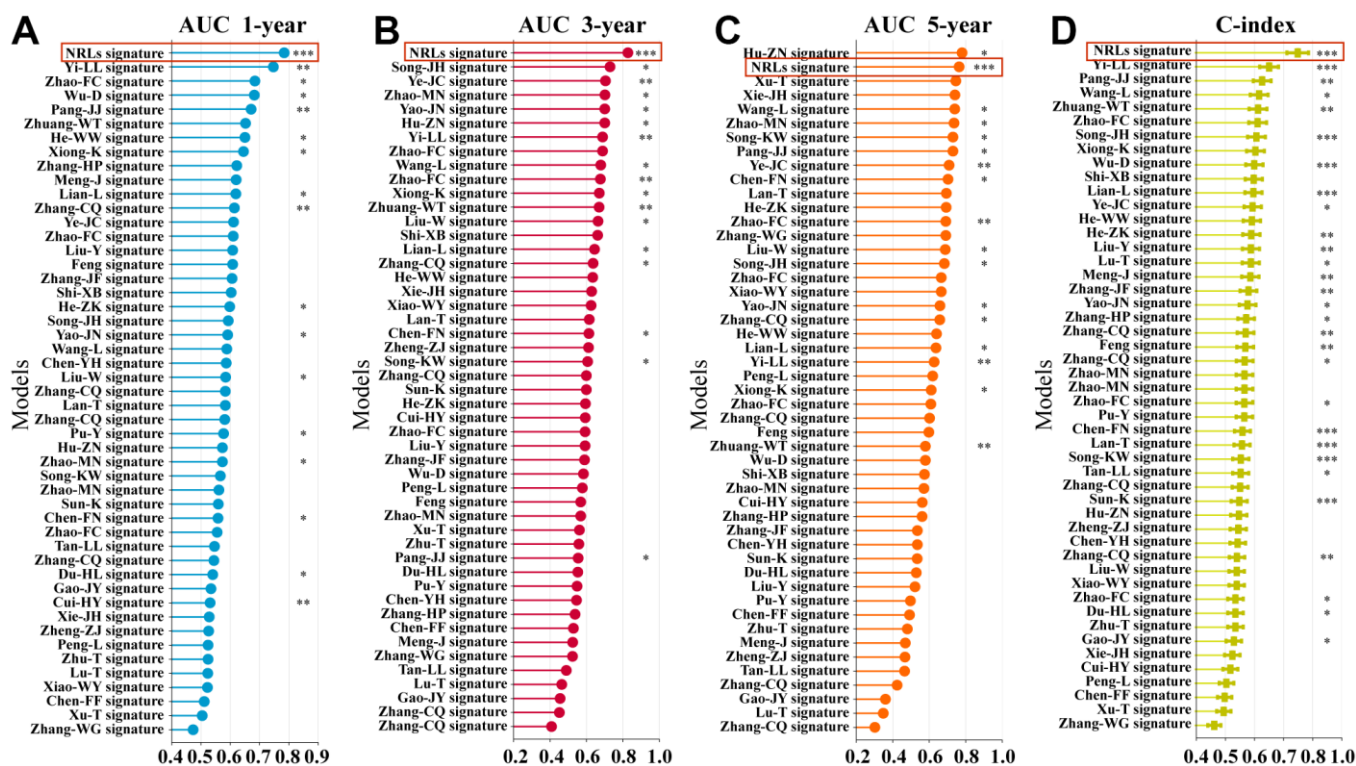

Figure 5. Comparison of multiple prognostic models. (**A–C**) Comparison of AUC in multiple prognostic models at 1-, 3-, and 5-year. (**D**) C-index comparison of six NRLs prognostic features with other prognostic features.
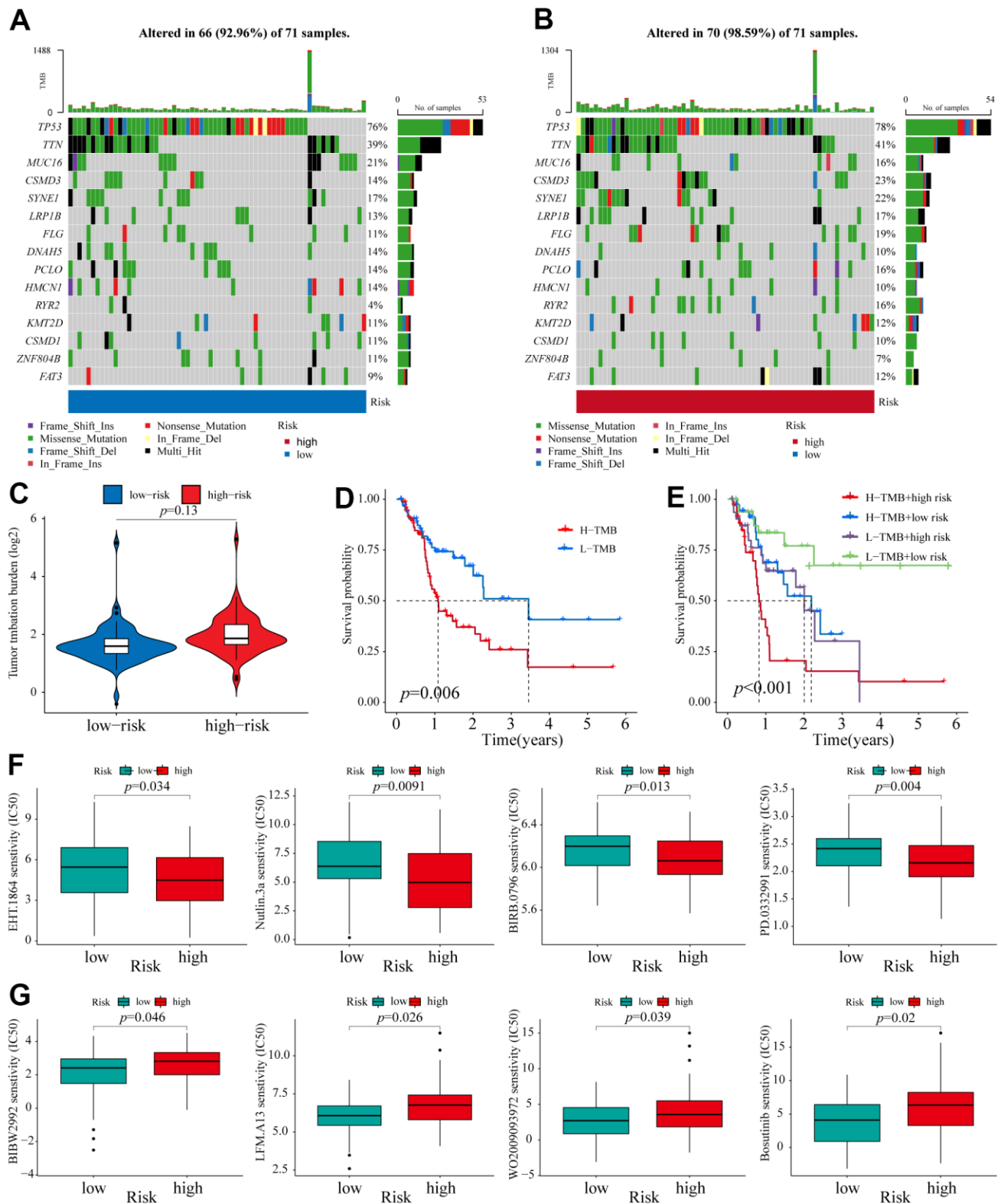
Figure 6. TMB analysis and Identification of potential compounds. (**A**, **B**) The waterfall plot of the mutation landscape of the top 15 genes with high mutation frequencies in the low- and high-risk groups. (**C**) TMB difference of patients in low- and high-risk groups. (**D**) Survival analysis for patients in high- and low-TMB. (**E**) Survival analysis for patients classified based on the TMB and 6-NRLs risk signature. The drug sensitivity of the high-risk group was higher than those of the low-risk group. (**F**) EHT.1864, Nutlin.3a, BIRB.0796, and PD.0332991. The drug sensitivity of the low-risk group was higher than those of the high-risk group. (**G**) BIBW2992, LFM.A13, WO2009093972, and Bosutinib.
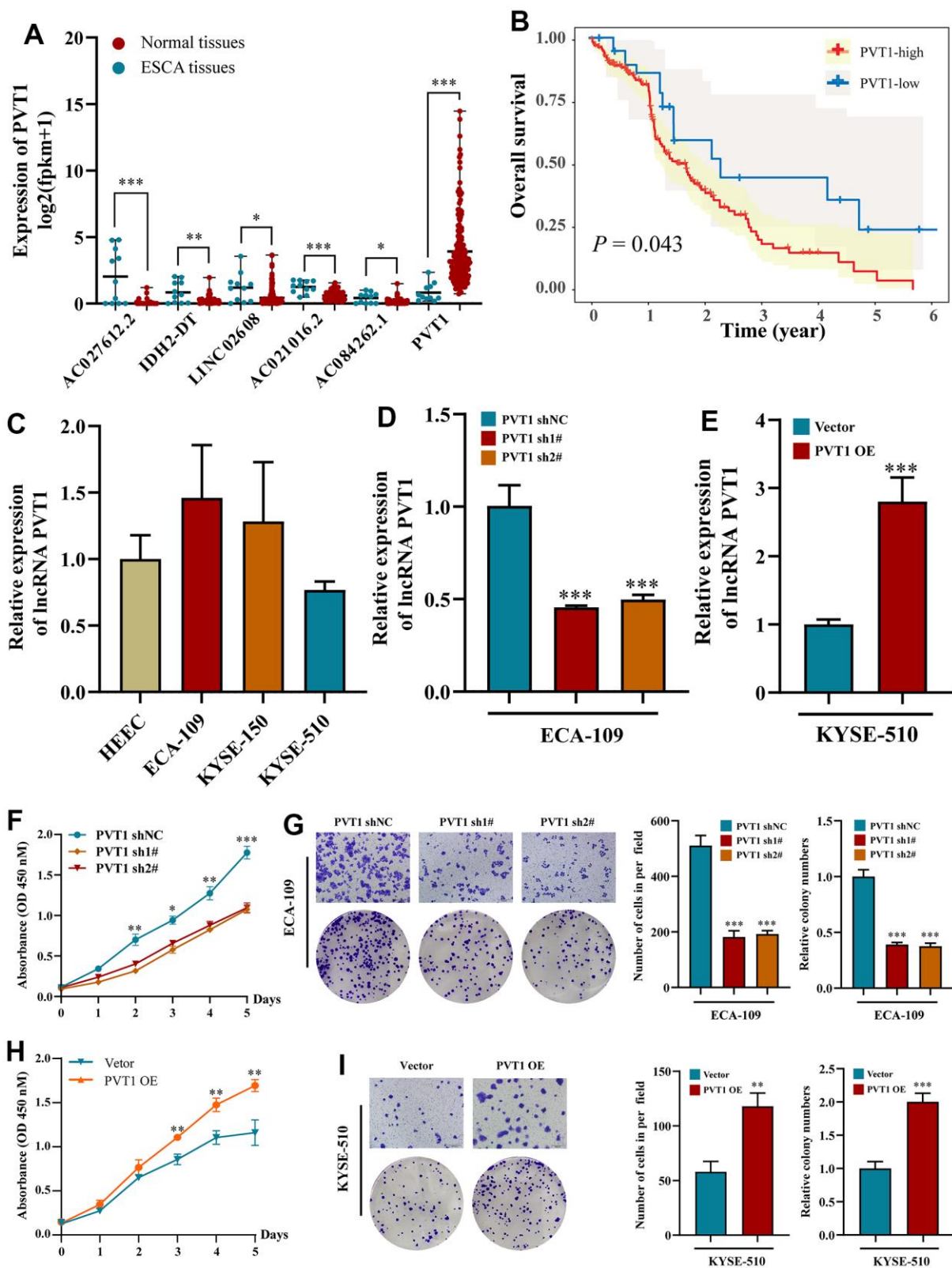
Figure 7. Effects of inhibiting the expression of PVT1 in cell proliferation and migration *in vitro*. (**A**) The expression of PVT1 in normal and ESCA tissues. (**B**) KM survival analysis for ESCA patients with different PVT1 expressions; (**C**) The expression of PVT1 in HEEC and ESCA cells; (**D**) The transfection efficiency of PVT1-sh1#/sh2# in ECA-150 cell; (**E**) The transfection efficiency of PVT1-OE in KYSE-510 cell; (**F**, **G**) Knockdown of PVT1 inhibited ECA-150 cell proliferation and colony formation ability. (**H**, **I**) Overexpression of PVT1 promoted KYSE-510 cell proliferation and colony formation ability. Data are presented as mean ± SD. (*p < 0.05, **p < 0.01, ***p < 0.001).

AC084262.1) based on LASSO and multi-Cox regression. Simultaneously, a nomogram, internal testing cohort, PCA, and TMB analysis were adopted to assess the validity of the prognostic panel. Besides, we further investigated the predictive capability of this prognostic model in various clinicopathological features and multiple prognostic signatures. The results showed that regardless of age, sex, grade, and other clinicopathologic indicators, the prognosis model could effectively divide ESCA patients into low- and high-risk groups. On the other hand, this 6-NRLs panel has more predictive power than other prognostic models. Overall, our results showed that the 6-NRLs prognostic panel had a good performance in predicting the prognosis of ESCA patients.

As one of the most common malignant tumors worldwide, ESCA originates from the esophageal mucosa epithelium. Some studies have confirmed that the dysregulation of lncRNAs is extensively involved in the biological processes of ESCA, including proliferation, apoptosis, metastasis, angiogenesis, and treatment resistance [19, 40, 41]. These findings indicate that lncRNAs have great clinical value and are candidate biomarkers for early diagnosis, treatment responses, and clinical outcomes. Although some lncRNA-related prognostic models in ESCA have been constructed, there is still a lack of effective evaluation of the prognostic models of ESCA [42–44]. Toll-like receptor (TLR) activates necroptosis through the interaction between TRIF and necrosome [45]. Liu et al. [46] have reported a promising 4-lncRNA prognostic signature for ESCA. In the present work, we identified 198 DE-NRLs between adjacent normal and ESCA tissues and constructed a 6-NRLs prognostic signature using LASSO-Cox regression. Among them, neither AC027612.2 nor
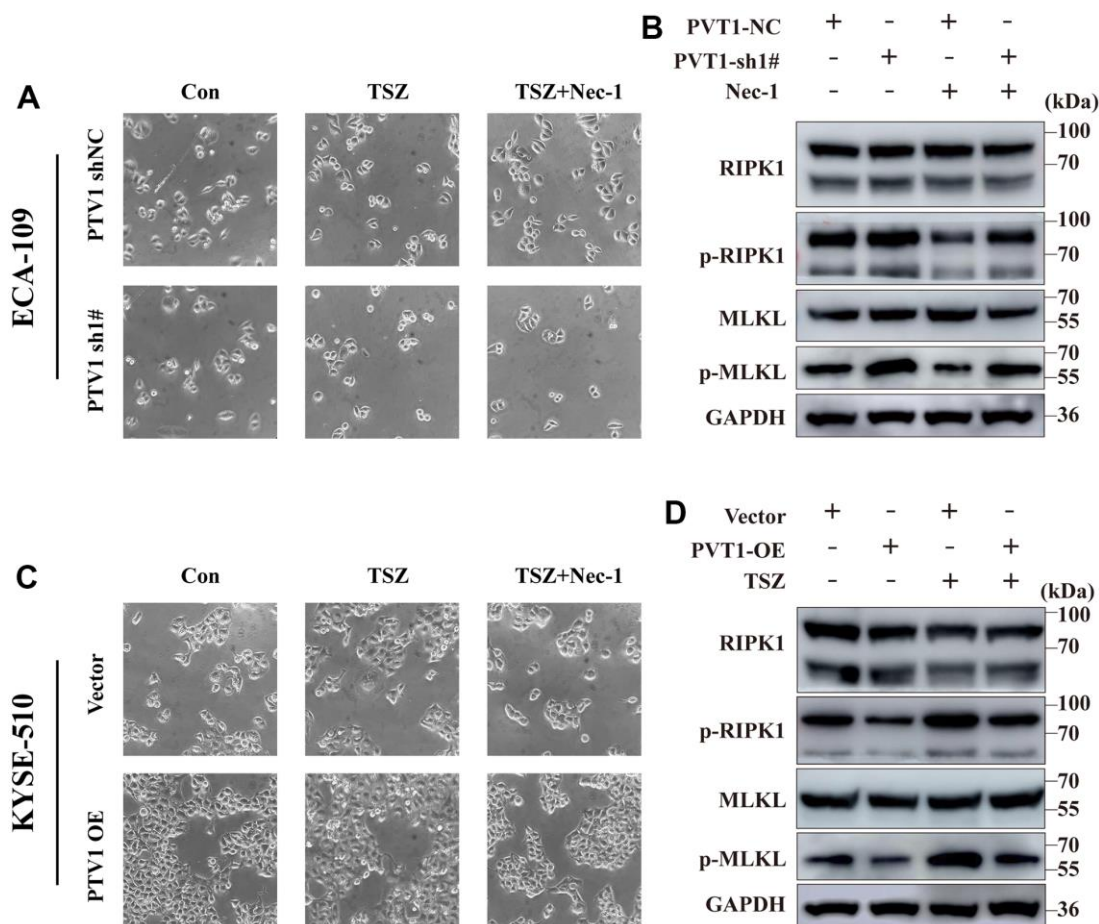
Figure 8. Induction of necroptotic cell death in PVT1-sh#/ PVT1-OE ESCA cells. (**A**) ECA-109 cells were treated with Nec-1 (50 μM) for 4 h and then treated with TSZ (30ng/ml TNF-α, 200nM Smac mimetics, 20μM zVAD). After 24 h of drug treatment, the morphological changes of treated cells were imaged under a phase-contrast microscope. (**B**) Western blot from ECA-109 cell was performed to detect RIP1, p-RIP1, MLKL, and p-MLKL protein levels. (**C**) KYSE-510 cells were treated with Nec-1 (50 μM) for 4 h and then treated with TSZ (30ng/ml TNF-α, 200nM Smac mimetics, 20μM zVAD). After 24 h of drug treatment, the morphological changes of treated cells were imaged under a phase-contrast microscope. (**D**) Western blot KYSE-510 cell was performed to detect RIP1, p-RIP1, MLKL, and p-MLKL protein levels.

LINC02608 have been previously reported in ESCA or other diseases. Studies have found that the combination of seven lncRNAs, including AC021016.2, AC079630.1, AC116407.1, and so on, can predict the prognosis of lung adenocarcinoma (LUAD) patients [47]. Interestingly, they have found that AC021016.2 also exhibits significant prognostic value in the validation cohort [47]. It has been reported that a prognostic scoring feature containing AC084262.1 has the potential to predict the clinical outcomes of ESCC, supporting our findings [48]. Increasing evidence has shown that IDH mutations have vital implications for the progression and treatment of various malignancies [49]. Zheng et al. [50] have found that wild-type IDH2 contributes to acute myeloid leukemia (AML) via inducing the conversion of α-KG to isocitrate for lipid synthesis and promoting c-Myc expression. These findings provide the possibility for targeting therapy of metabolic vulnerability. Additionally, it seems that the combination of enasidenib and azacitidine can be used as a feasible strategy for treating AML patients harboring IDH2 mutations [51]. Furthermore, previous reports have confirmed that PVT1 is widely involved in the proliferation, invasion, metastasis, and multidrug resistance of digestive tract tumor cells, such as esophageal adenocarcinoma [52], colorectal cancer [53], gallbladder cancer [54], and pancreatic cancer [55]. Numerous evidences have revealed that exosomal non-coding RNAs have significant clinical values in disease diagnosis and prognosis, and have become one of that new frontier biomarkers of cancer liquid biopsy [56]. Studies shown that aberrant expression of exosomal lncRNA PVT1 may contribute to disease progression [57, 58]. Collectively, PVT1 has become an emerging biomarker for early screening, efficacy evaluation, and prognostic prediction. Nevertheless, though many efforts have been made in NRLs research, the underlying mechanisms of NRLs in ESCA remain largely unexplored.

To further investigate the underlying molecular mechanisms of the signature, the GSEA was carried out between different risk groups. The signaling pathways related to metabolisms, such as the TCA cycle, ribosome, glycosaminoglycan degradation, mTOR signaling pathway, and primary bile acid biosynthesis, were mainly enriched in the high-risk group. Conversely, TGF, notch, pentose phosphate, and Hedgehog pathways were enriched in the low-risk group. It has been found that the inhibition of mito-chondrial oxidative phosphorylation mediated via clomipramine helps restrain ESCC progression [59]. The mutations of key regulators in the mTOR pathway significantly affect the survival and prognosis of cancer patients [60]. Studies have shown that ipriflavone and apatinib enhance the chemosensitivity of ESCC through mTOR-related signaling pathways

[61, 62]. Furthermore, notch and Hedgehog pathways are associated with the radioresistance of ESCC [63]. Finally, we predicted some compounds that might be used to treat patients of different risk groups. For instance, Nutlin.3a (Rebemadlin) is an effective MDM2 inhibitor, and inhibition of MDM2 can stabilize p53 protein and thus induce autophagy and apoptosis [64]. Our results indicate that high-risk ESCA patients may be more sensitive to Nutlin.3a (Figure 6F), suggesting that Nutlin.3a could be used as a treatment for these patients. Taken together, these findings supported better individualized therapeutic strategies for ESCA patients.

In addition, the functional phenotype of PVT1 in ESCA cell lines was explored through experimental studies. We first verified the expression level of PVT1 from the TCGA database and cell lines. *In vitro* analysis revealed that overexpression of PVT1 facilitated the pro-liferation, migration, and colony formation in ESCA cells, and depletion of PVT1 effectively alleviated this phenotype. Interestingly, inhibiting PVT1 increased the expressions of p-RIP1 and p-MLKL and enhanced necroptosis, suggesting that PVT1 was a potential NRLs in ESCA.

However, our research has some limitations. First, our results were mainly based on the TCGA dataset. Therefore, other large-scale case series data and clinical samples for external verification are required to further evaluate the applicability of the signature. Second, we only verified that PVT1 was a possible oncogenic lncRNA, while the specific mechanism of necroptosis regulating ESCA is still unclear, and the remaining NRGs and NRLs and more detailed molecular mechanisms need to be further proved via *in vitro* and *in vivo* experiments.

CONCLUSIONS

In this study, we constructed a promising prognostic panel consisting of six NRLs, which was not only an independent predictor but also a potential therapeutic target. Furthermore, we also found that PVT1 was a potential regulator of necroptosis, and it participated in the development of ESCA. Collectively, our current findings provided valuable insights into the tumor progression and clinical outcomes of ESCA patients.

Abbreviations

ESCA: esophageal carcinoma; ESCC: esophageal squamous cell carcinoma; lncRNAs: long non-coding RNAs; NRLs: necroptosis-related lncRNAs; NRGs: necroptosis-related genes; DE-NRGs: differentially expressed necroptosis-related genes; DE-NRLs: differentially expressed necroptosis-related lncRNAs;

TCGA: the Cancer Genome Atlas; TNF-α: tumor necrosis factor-α; RIPK1: receptor interacting protein-1; RIPK3: receptor-interacting protein kinase 3; MLKL: mixed-lineage kinase domain-like protein; CCRT: concurrent chemoradiotherapy; CeRNA: competing endogenous RNA; LASSO: least absolute shrinkage and selection operator; PCA: principal component analysis; ROC: receiver operating characteristic; C-index: concordance index; TMB: tumor mutational burden; GSEA: gene set enrichment analysis; NRGs: necroptosis-related genes; KEGG: Kyoto Encyclopedia of Genes and Genomes; DE-NRGs: differentially expressed NRGs; OS: the overall survival; PPI: protein-protein interaction; IC50: half-maximal inhibitory concentration; AUCs: the area under ROC curves; TLR: Toll-like receptor; AML: acute myeloid leukemia; LUAD: lung adenocarcinoma.

AUTHOR CONTRIBUTIONS

Yi Zhang and Xin Zhang conceptualized the study and contributed to funding acquisition; Zhengdong Luo and E Ding performed bioinformatics analysis and wrote the original draft; Longchen Yu, Wenwu Wang, Qining Guo, and Xinyang Li helped in the investigation, formal analysis, methodology, and experimental verification; Yifeng Wang and Tingting Li curated the data; Xin Zhang contributed to supervising, writing, review and editing. All authors contributed to the study and approved the final manuscript.

CONFLICTS OF INTEREST

The authors declare that they have no conflicts of interest.

FUNDING

REFERENCES

1. Thrift AP. Global burden and epidemiology of Barrett oesophagus and oesophageal cancer. Nat Rev Gastroenterol Hepatol. 2021; 18:432–43. https://doi.org/10.1038/s41575-021-00419-3 PMID:33603224

2. Sung H, Ferlay J, Siegel RL, Laversanne M, Soerjomataram I, Jemal A, Bray F. Global Cancer Statistics 2020: GLOBOCAN Estimates of Incidence and Mortality Worldwide for 36 Cancers in 185 Countries. CA Cancer J Clin. 2021; 71:209–49. https://doi.org/10.3322/caac.21660 PMID:33538338

3. Maret-Ouda J, Santoni G, Wahlin K, Artama M, Brusselaers N, Färkkilä M, Lynge E, Mattsson F, Pukkala E, Romundstad P, Tryggvadóttir L, von Euler-Chelpin M, Lagergren J. Esophageal Adenocarcinoma After Antireflux Surgery in a Cohort Study From the 5 Nordic Countries. Ann Surg. 2021; 274:e535–40. https://doi.org/10.1097/SLA.0000000000003709 PMID:31800492

4. Kelly RJ. Emerging Multimodality Approaches to Treat Localized Esophageal Cancer. J Natl Compr Canc Netw. 2019; 17:1009–14. https://doi.org/10.6004/jnccn.2019.7337 PMID:31390584

5. Eyck BM, van Lanschot JJB, Hulshof MCCM, van der Wilk BJ, Shapiro J, van Hagen P, van Berge Henegouwen MI, Wijnhoven BPL, van Laarhoven HWM, Nieuwenhuijzen GAP, Hospers GAP, Bonenkamp JJ, Cuesta MA, et al, and CROSS Study Group. Ten-Year Outcome of Neoadjuvant Chemoradiotherapy Plus Surgery for Esophageal Cancer: The Randomized Controlled CROSS Trial. J Clin Oncol. 2021; 39:1995–2004. https://doi.org/10.1200/JCO.20.03614 PMID:33891478

6. Kelly RJ, Ajani JA, Kuzdzal J, Zander T, Van Cutsem E, Piessen G, Mendez G, Feliciano J, Motoyama S, Lièvre A, Uronis H, Elimova E, Grootscholten C, et al, and CheckMate 577 Investigators. Adjuvant Nivolumab in Resected Esophageal or Gastroesophageal Junction Cancer. N Engl J Med. 2021; 384:1191–203. https://doi.org/10.1056/NEJMoa2032125 PMID:33789008

7. Yamamoto S, Kato K. JUPITER-06 establishes immune checkpoint inhibitors as essential first-line drugs for the treatment of advanced esophageal squamous cell carcinoma. Cancer Cell. 2022; 40:238–40. https://doi.org/10.1016/j.ccell.2022.02.009 PMID:35245448

8. Cho YS, Challa S, Moquin D, Genga R, Ray TD, Guildford M, Chan FK. Phosphorylation-driven assembly of the RIP1-RIP3 complex regulates programmed necrosis and virus-induced inflammation. Cell. 2009; 137:1112–23. https://doi.org/10.1016/j.cell.2009.05.037 PMID:19524513

9. Linkermann A, Green DR. Necroptosis. N Engl J Med. 2014; 370:455–65. https://doi.org/10.1056/NEJMra1310050 PMID:24476434

10. Galluzzi L, Vitale I, Aaronson SA, Abrams JM, Adam D, Agostinis P, Alnemri ES, Altucci L, Amelio I, Andrews DW, Annicchiarico-Petruzzelli M, Antonov AV,

Arama E, et al. Molecular mechanisms of cell death: recommendations of the Nomenclature Committee on Cell Death 2018. Cell Death Differ. 2018; 25:486–541.
https://doi.org/10.1038/s41418-017-0012-4
PMID:29362479

11. Najafov A, Chen H, Yuan J. Necroptosis and Cancer. Trends Cancer. 2017; 3:294–301.
https://doi.org/10.1016/j.trecan.2017.03.002
PMID:28451648

12. Gong Y, Fan Z, Luo G, Yang C, Huang Q, Fan K, Cheng H, Jin K, Ni Q, Yu X, Liu C. The role of necroptosis in cancer biology and therapy. Mol Cancer. 2019; 18:100.
https://doi.org/10.1186/s12943-019-1029-8
PMID:31122251

13. Aaes TL, Kaczmarek A, Delvaeye T, De Craene B, De Koker S, Heyndrickx L, Delrue I, Taminau J, Wiernicki B, De Groote P, Garg AD, Leybaert L, Grooten J, et al. Vaccination with Necroptotic Cancer Cells Induces Efficient Anti-tumor Immunity. Cell Rep. 2016; 15:274–87.
https://doi.org/10.1016/j.celrep.2016.03.037
PMID:27050509

14. Zheng ZY, Yang PL, Luo W, Yu SX, Xu HY, Huang Y, Li RY, Chen Y, Xu XE, Liao LD, Wang SH, Huang HC, Li EM, Xu LY. STAT3β Enhances Sensitivity to Concurrent Chemoradiotherapy by Inducing Cellular Necroptosis in Esophageal Squamous Cell Carcinoma. Cancers (Basel). 2021; 13:901.
https://doi.org/10.3390/cancers13040901
PMID:33670049

15. Yamauchi T, Fujishima F, Hashimoto M, Tsunokake J, Akaishi R, Gokon Y, Ueki S, Ozawa Y, Fukutomi T, Okamoto H, Sato C, Taniyama Y, Nakamura T, et al. Necroptosis in Esophageal Squamous Cell Carcinoma: An Independent Prognostic Factor and Its Correlation with Tumor-Infiltrating Lymphocytes. Cancers (Basel). 2021; 13:4473.
https://doi.org/10.3390/cancers13174473
PMID:34503283

16. Guttman M, Amit I, Garber M, French C, Lin MF, Feldser D, Huarte M, Zuk O, Carey BW, Cassady JP, Cabili MN, Jaenisch R, Mikkelsen TS, et al. Chromatin signature reveals over a thousand highly conserved large non-coding RNAs in mammals. Nature. 2009; 458:223–7.
https://doi.org/10.1038/nature07672 PMID:19182780

17. Engreitz JM, Haines JE, Perez EM, Munson G, Chen J, Kane M, McDonel PE, Guttman M, Lander ES. Local regulation of gene expression by lncRNA promoters, transcription and splicing. Nature. 2016; 539:452–5.
https://doi.org/10.1038/nature20149
PMID:27783602

18. Nojima T, Proudfoot NJ. Mechanisms of lncRNA biogenesis as revealed by nascent transcriptomics. Nat Rev Mol Cell Biol. 2022; 23:389–406.
https://doi.org/10.1038/s41580-021-00447-6
PMID:35079163

19. Abraham JM, Meltzer SJ. Long Noncoding RNAs in the Pathogenesis of Barrett's Esophagus and Esophageal Carcinoma. Gastroenterology. 2017; 153:27–34.
https://doi.org/10.1053/j.gastro.2017.04.046
PMID:28528706

20. Xue ST, Zheng B, Cao SQ, Ding JC, Hu GS, Liu W, Chen C. Long non-coding RNA LINC00680 functions as a ceRNA to promote esophageal squamous cell carcinoma progression through the miR-423-5p/PAK6 axis. Mol Cancer. 2022; 21:69.
https://doi.org/10.1186/s12943-022-01539-3
PMID:35255921

21. Wang Y, Zhang W, Liu W, Huang L, Wang Y, Li D, Wang G, Zhao Z, Chi X, Xue Y, Song Y, Liu X, Zhan Q. Long Noncoding RNA VESTAR Regulates Lymphangiogenesis and Lymph Node Metastasis of Esophageal Squamous Cell Carcinoma by Enhancing VEGFC mRNA Stability. Cancer Res. 2021; 81:3187–99.
https://doi.org/10.1158/0008-5472.CAN-20-1713
PMID:33771898

22. Liang Y, Chen X, Wu Y, Li J, Zhang S, Wang K, Guan X, Yang K, Bai Y. LncRNA CASC9 promotes esophageal squamous cell carcinoma metastasis through upregulating LAMC2 expression by interacting with the CREB-binding protein. Cell Death Differ. 2018; 25:1980–95.
https://doi.org/10.1038/s41418-018-0084-9
PMID:29511340

23. Lu Y, Luo X, Wang Q, Chen J, Zhang X, Li Y, Chen Y, Li X, Han S. A Novel Necroptosis-Related lncRNA Signature Predicts the Prognosis of Lung Adenocarcinoma. Front Genet. 2022; 13:862741.
https://doi.org/10.3389/fgene.2022.862741
PMID:35368663

24. Luo L, Li L, Liu L, Feng Z, Zeng Q, Shu X, Cao Y, Li Z. A Necroptosis-Related lncRNA-Based Signature to Predict Prognosis and Probe Molecular Characteristics of Stomach Adenocarcinoma. Front Genet. 2022; 13:833928.
https://doi.org/10.3389/fgene.2022.833928
PMID:35330731

25. Liu L, Huang L, Chen W, Zhang G, Li Y, Wu Y, Xiong J, Jie Z. Comprehensive Analysis of Necroptosis-Related Long Noncoding RNA Immune Infiltration and Prediction of Prognosis in Patients With Colon Cancer. Front Mol Biosci. 2022; 9:811269.
https://doi.org/10.3389/fmolb.2022.811269
PMID:35237659

26. Wang Y, Chen W, Lian J, Zhang H, Yu B, Zhang M, Wei F, Wu J, Jiang J, Jia Y, Mo F, Zhang S, Liang X, et al. The lncRNA PVT1 regulates nasopharyngeal carcinoma cell proliferation via activating the KAT2A acetyltransferase and stabilizing HIF-1α. Cell Death Differ. 2020; 27:695–710.
https://doi.org/10.1038/s41418-019-0381-y
PMID:31320749

27. Guo H, Zhuang K, Ding N, Hua R, Tang H, Wu Y, Yuan Z, Li T, He S. High-fat diet induced cyclophilin B enhances STAT3/lncRNA-PVT1 feedforward loop and promotes growth and metastasis in colorectal cancer. Cell Death Dis. 2022; 13:883.
https://doi.org/10.1038/s41419-022-05328-0
PMID:36266267

28. Chen Y, Li F, Li D, Liu W, Zhang L. Atezolizumab and blockade of LncRNA PVT1 attenuate cisplatin resistant ovarian cancer cells progression synergistically via JAK2/STAT3/PD-L1 pathway. Clin Immunol. 2021; 227:108728.
https://doi.org/10.1016/j.clim.2021.108728
PMID:33878452

29. Li R, Wang X, Zhu C, Wang K. lncRNA PVT1: a novel oncogene in multiple cancers. Cell Mol Biol Lett. 2022; 27:84.
https://doi.org/10.1186/s11658-022-00385-x
PMID:36195846

30. Zhang MX, Zhang LZ, Fu LM, Yao HH, Tan L, Feng ZH, Li JY, Lu J, Pan YH, Shu GN, Li PJ, Tang YM, Liao ZY, et al. Positive feedback regulation of lncRNA PVT1 and HIF2α contributes to clear cell renal cell carcinoma tumorigenesis and metastasis. Oncogene. 2021; 40:5639–50.
https://doi.org/10.1038/s41388-021-01971-7
PMID:34321604

31. Liu S, Chen W, Hu H, Zhang T, Wu T, Li X, Li Y, Kong Q, Lu H, Lu Z. Long noncoding RNA PVT1 promotes breast cancer proliferation and metastasis by binding miR-128-3p and UPF1. Breast Cancer Res. 2021; 23:115.
https://doi.org/10.1186/s13058-021-01491-y
PMID:34922601

32. Sun Y, Ren D, Zhou Y, Shen J, Wu H, Jin X. Histone acetyltransferase 1 promotes gemcitabine resistance by regulating the PVT1/EZH2 complex in pancreatic cancer. Cell Death Dis. 2021; 12:878.
https://doi.org/10.1038/s41419-021-04118-4
PMID:34564701

33. Yamamoto A, Kurata M, Yamamoto K, Nogawa D, Inoue M, Ishibashi S, Ikeda M, Miyasaka N, Kitagawa M. High amplification of PVT1 and MYC predict favorable prognosis in early ovarian carcinoma. Pathol Res Pract. 2020; 216:153175.
https://doi.org/10.1016/j.prp.2020.153175
PMID:32841774

34. Park JH, Jung KH, Kim SJ, Yoon YC, Yan HH, Fang Z, Lee JE, Lim JH, Mah S, Hong S, Kim YS, Hong SS. HS-173 as a novel inducer of RIP3-dependent necroptosis in lung cancer. Cancer Lett. 2019; 444:94–104.
https://doi.org/10.1016/j.canlet.2018.12.006
PMID:30583075

35. Passaro A, Stenzinger A, Peters S. Tumor Mutational Burden as a Pan-cancer Biomarker for Immunotherapy: The Limits and Potential for Convergence. Cancer Cell. 2020; 38:624–5.
https://doi.org/10.1016/j.ccell.2020.10.019
PMID:33171127

36. Valero C, Lee M, Hoen D, Wang J, Nadeem Z, Patel N, Postow MA, Shoushtari AN, Plitas G, Balachandran VP, Smith JJ, Crago AM, Long Roche KC, et al. The association between tumor mutational burden and prognosis is dependent on treatment context. Nat Genet. 2021; 53:11–5.
https://doi.org/10.1038/s41588-020-00752-4
PMID:33398197

37. Snyder AG, Oberst A. The Antisocial Network: Cross Talk Between Cell Death Programs in Host Defense. Annu Rev Immunol. 2021; 39:77–101.
https://doi.org/10.1146/annurev-immunol-112019-072301 PMID:33441019

38. Yan J, Wan P, Choksi S, Liu ZG. Necroptosis and tumor progression. Trends Cancer. 2022; 8:21–7.
https://doi.org/10.1016/j.trecan.2021.09.003
PMID:34627742

39. Cao K, Tait SW. Parkin inhibits necroptosis to prevent cancer. Nat Cell Biol. 2019; 21:915–6.
https://doi.org/10.1038/s41556-019-0350-1
PMID:31358970

40. Su M, Xiao Y, Ma J, Cao D, Zhou Y, Wang H, Liao Q, Wang W. Long non-coding RNAs in esophageal cancer: molecular mechanisms, functions, and potential applications. J Hematol Oncol. 2018; 11:118.
https://doi.org/10.1186/s13045-018-0663-8
PMID:30223861

41. Xue W, Zheng Y, Shen Z, Li L, Fan Z, Wang W, Zhu Z, Zhai Y, Zhao J, Kan Q. Involvement of long non-coding RNAs in the progression of esophageal cancer. Cancer Commun (Lond). 2021; 41:371–88.
https://doi.org/10.1002/cac2.12146
PMID:33605567

42. Zhu T, Ma Z, Wang H, Wei D, Wang B, Zhang C, Fu L, Li Z, Yu G. Immune-Related Long Non-coding RNA Signature and Clinical Nomogram to Evaluate Survival of Patients Suffering Esophageal Squamous Cell Carcinoma. Front Cell Dev Biol. 2021; 9:641960.

https://doi.org/10.3389/fcell.2021.641960
PMID:33748133

43. Hu X, Wu L, Liu B, Chen K. Immune Infiltration Subtypes Characterization and Identification of Prognosis-Related lncRNAs in Adenocarcinoma of the Esophagogastric Junction. Front Immunol. 2021; 12:651056.
https://doi.org/10.3389/fimmu.2021.651056
PMID:34122409

44. Zheng ZJ, Li YS, Zhu JD, Zou HY, Fang WK, Cui YY, Xie JJ. Construction of the Six-lncRNA Prognosis Signature as a Novel Biomarker in Esophageal Squamous Cell Carcinoma. Front Genet. 2022; 13:839589.
https://doi.org/10.3389/fgene.2022.839589
PMID:35432441

45. Kaiser WJ, Sridharan H, Huang C, Mandal P, Upton JW, Gough PJ, Sehon CA, Marquis RW, Bertin J, Mocarski ES. Toll-like receptor 3-mediated necrosis via TRIF, RIP3, and MLKL. J Biol Chem. 2013; 288:31268–79.
https://doi.org/10.1074/jbc.M113.462341
PMID:24019532

46. Liu J, Wang Y, Chu Y, Xu R, Zhang D, Wang X. Identification of a TLR-Induced Four-lncRNA Signature as a Novel Prognostic Biomarker in Esophageal Carcinoma. Front Cell Dev Biol. 2020; 8:649.
https://doi.org/10.3389/fcell.2020.00649
PMID:32850794

47. Hou J, Yao C. Potential Prognostic Biomarkers of Lung Adenocarcinoma Based on Bioinformatic Analysis. Biomed Res Int. 2021; 2021:8859996.
https://doi.org/10.1155/2021/8859996
PMID:33511215

48. Shi X, Li Y, Sun Y, Zhao X, Sun X, Gong T, Liang Z, Ma Y, Zhang X. Genome-wide analysis of lncRNAs, miRNAs, and mRNAs forming a prognostic scoring system in esophageal squamous cell carcinoma. PeerJ. 2020; 8:e8368.
https://doi.org/10.7717/peerj.8368 PMID:32095316

49. Pirozzi CJ, Yan H. The implications of IDH mutations for cancer development and therapy. Nat Rev Clin Oncol. 2021; 18:645–61.
https://doi.org/10.1038/s41571-021-00521-0
PMID:34131315

50. Zeng P, Lu W, Tian J, Qiao S, Li J, Glorieux C, Wen S, Zhang H, Li Y, Huang P. Reductive TCA cycle catalyzed by wild-type IDH2 promotes acute myeloid leukemia and is a metabolic vulnerability for potential targeted therapy. J Hematol Oncol. 2022; 15:30.
https://doi.org/10.1186/s13045-022-01245-z
PMID:35313945

51. Venugopal S, Takahashi K, Daver N, Maiti A, Borthakur G, Loghavi S, Short NJ, Ohanian M, Masarova L, Issa G,

Wang X, Carlos BR, Yilmaz M, et al. Efficacy and safety of enasidenib and azacitidine combination in patients with IDH2 mutated acute myeloid leukemia and not eligible for intensive chemotherapy. Blood Cancer J. 2022; 12:10.
https://doi.org/10.1038/s41408-021-00604-2
PMID:35078972

52. Xu Y, Li Y, Jin J, Han G, Sun C, Pizzi MP, Huo L, Scott A, Wang Y, Ma L, Lee JH, Bhutani MS, Weston B, et al. LncRNA PVT1 up-regulation is a poor prognosticator and serves as a therapeutic target in esophageal adenocarcinoma. Mol Cancer. 2019; 18:141.
https://doi.org/10.1186/s12943-019-1064-5
PMID:31601234

53. Shigeyasu K, Toden S, Ozawa T, Matsuyama T, Nagasaka T, Ishikawa T, Sahoo D, Ghosh P, Uetake H, Fujiwara T, Goel A. The PVT1 lncRNA is a novel epigenetic enhancer of MYC, and a promising risk-stratification biomarker in colorectal cancer. Mol Cancer. 2020; 19:155.
https://doi.org/10.1186/s12943-020-01277-4
PMID:33148262

54. Chen J, Yu Y, Li H, Hu Q, Chen X, He Y, Xue C, Ren F, Ren Z, Li J, Liu L, Duan Z, Cui G, Sun R. Long non-coding RNA PVT1 promotes tumor progression by regulating the miR-143/HK2 axis in gallbladder cancer. Mol Cancer. 2019; 18:33.
https://doi.org/10.1186/s12943-019-0947-9
PMID:30825877

55. Zhou C, Yi C, Yi Y, Qin W, Yan Y, Dong X, Zhang X, Huang Y, Zhang R, Wei J, Ali DW, Michalak M, Chen XZ, Tang J. LncRNA PVT1 promotes gemcitabine resistance of pancreatic cancer via activating Wnt/β-catenin and autophagy pathway through modulating the miR-619-5p/Pygo2 and miR-619-5p/ATG14 axes. Mol Cancer. 2020; 19:118.
https://doi.org/10.1186/s12943-020-01237-y
PMID:32727463

56. Baassiri A, Nassar F, Mukherji D, Shamseddine A, Nasr R, Temraz S. Exosomal Non Coding RNA in LIQUID Biopsies as a Promising Biomarker for Colorectal Cancer. Int J Mol Sci. 2020; 21:1398.
https://doi.org/10.3390/ijms21041398 PMID:32092975

57. Lai SW, Chen MY, Bamodu OA, Hsieh MS, Huang TY, Yeh CT, Lee WH, Cherng YG. Exosomal lncRNA PVT1/VEGFA Axis Promotes Colon Cancer Metastasis and Stemness by Downregulation of Tumor Suppressor miR-152-3p. Oxid Med Cell Longev. 2021; 2021:9959807.
https://doi.org/10.1155/2021/9959807
PMID:34336125

58. Sun C, Wang P, Dong W, Liu H, Sun J, Zhao L. LncRNA PVT1 promotes exosome secretion through YKT6,

RAB7, and VAMP3 in pancreatic cancer. Aging (Albany NY). 2020; 12:10427–40.
https://doi.org/10.18632/aging.103268
PMID:32499447

59. Li B, Yu Y, Jiang Y, Zhao L, Li A, Li M, Yuan B, Lu J, Dong Z, Zhao J, Liu K. Cloperastine inhibits esophageal squamous cell carcinoma proliferation *in vivo* and *in vitro* by suppressing mitochondrial oxidative phosphorylation. Cell Death Discov. 2021; 7:166.
https://doi.org/10.1038/s41420-021-00509-w
PMID:34226508

60. Luo Q, Du R, Liu W, Huang G, Dong Z, Li X. PI3K/Akt/mTOR Signaling Pathway: Role in Esophageal Squamous Cell Carcinoma, Regulatory Mechanisms and Opportunities for Targeted Therapy. Front Oncol. 2022; 12:852383.
https://doi.org/10.3389/fonc.2022.852383
PMID:35392233

61. Shi X, Zhang Y, Xie X, Pang M, Laster K, Li J, Ma X, Liu K, Dong Z, Kim DJ. Ipriflavone Suppresses Growth of Esophageal Squamous Cell Carcinoma Through Inhibiting mTOR *In Vitro* and *In Vivo*. Front Oncol. 2021; 11:648809.
https://doi.org/10.3389/fonc.2021.648809
PMID:34178634

62. Wang YM, Xu X, Tang J, Sun ZY, Fu YJ, Zhao XJ, Ma XM, Ye Q. Apatinib induces endoplasmic reticulum stress-mediated apoptosis and autophagy and potentiates cell sensitivity to paclitaxel via the IRE-1α-AKT-mTOR pathway in esophageal squamous cell carcinoma. Cell Biosci. 2021; 11:124.
https://doi.org/10.1186/s13578-021-00640-2
PMID:34229754

63. Zhang H, Si J, Yue J, Ma S. The mechanisms and reversal strategies of tumor radioresistance in esophageal squamous cell carcinoma. J Cancer Res Clin Oncol. 2021; 147:1275–86.
https://doi.org/10.1007/s00432-020-03493-3
PMID:33687564

64. Chen Y, Xin H, Peng H, Shi Q, Li M, Yu J, Tian Y, Han X, Chen X, Zheng Y, Li J, Yang Z, Yang L, et al. Hypomethylation-Linked Activation of PLCE1 Impedes Autophagy and Promotes Tumorigenesis through MDM2-Mediated Ubiquitination and Destabilization of p53. Cancer Res. 2020; 80:2175–89.
https://doi.org/10.1158/0008-5472.CAN-19-1912
PMID:32066565
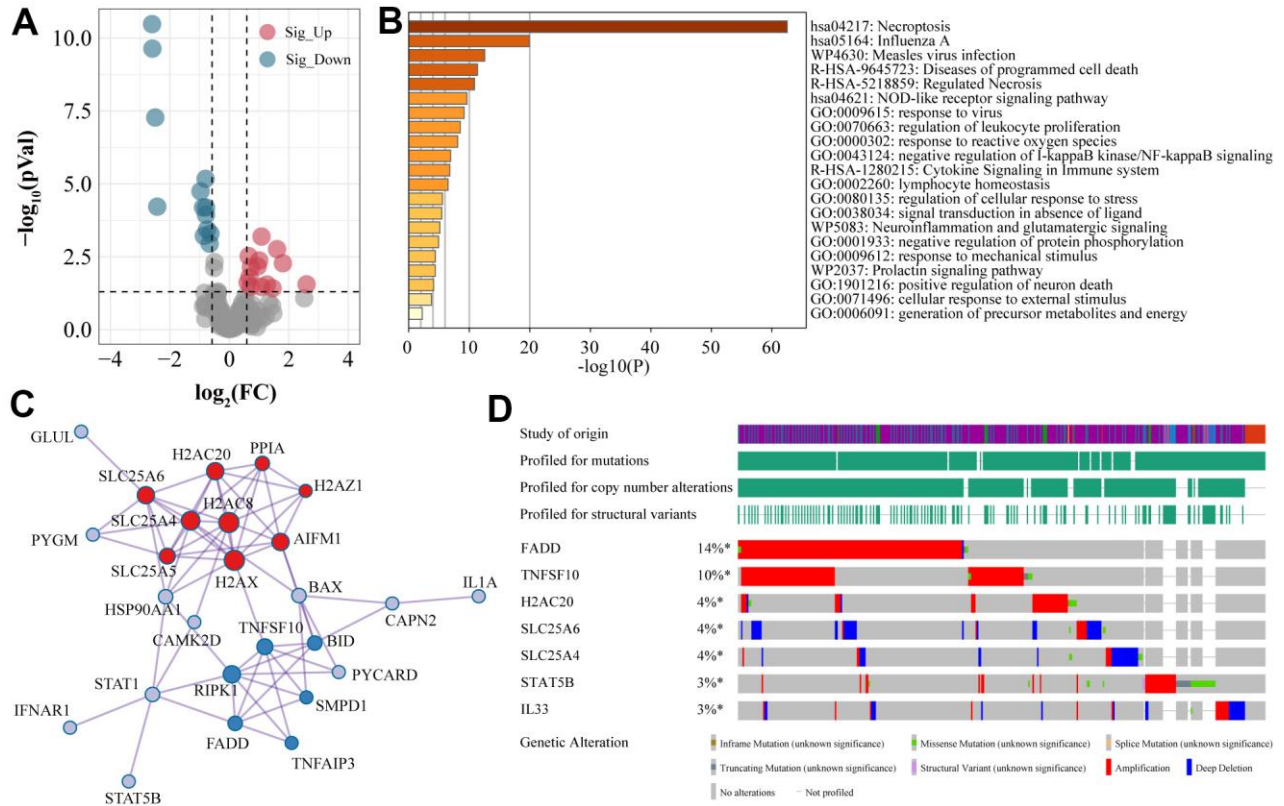
Supplementary Figure 1. The differentially expressed, interaction, and mutation analysis of NRGs. (**A**) The volcano plot of the significantly different expression of NRGs in ESCA and adjacent tissues. (**B**) KEGG enrichment analysis of differentially expressed NRGs. (**C**) A PPI network showed interactions of NRGs. (**D**) A total of seven NRGs has a mutation rate of ≥3%.
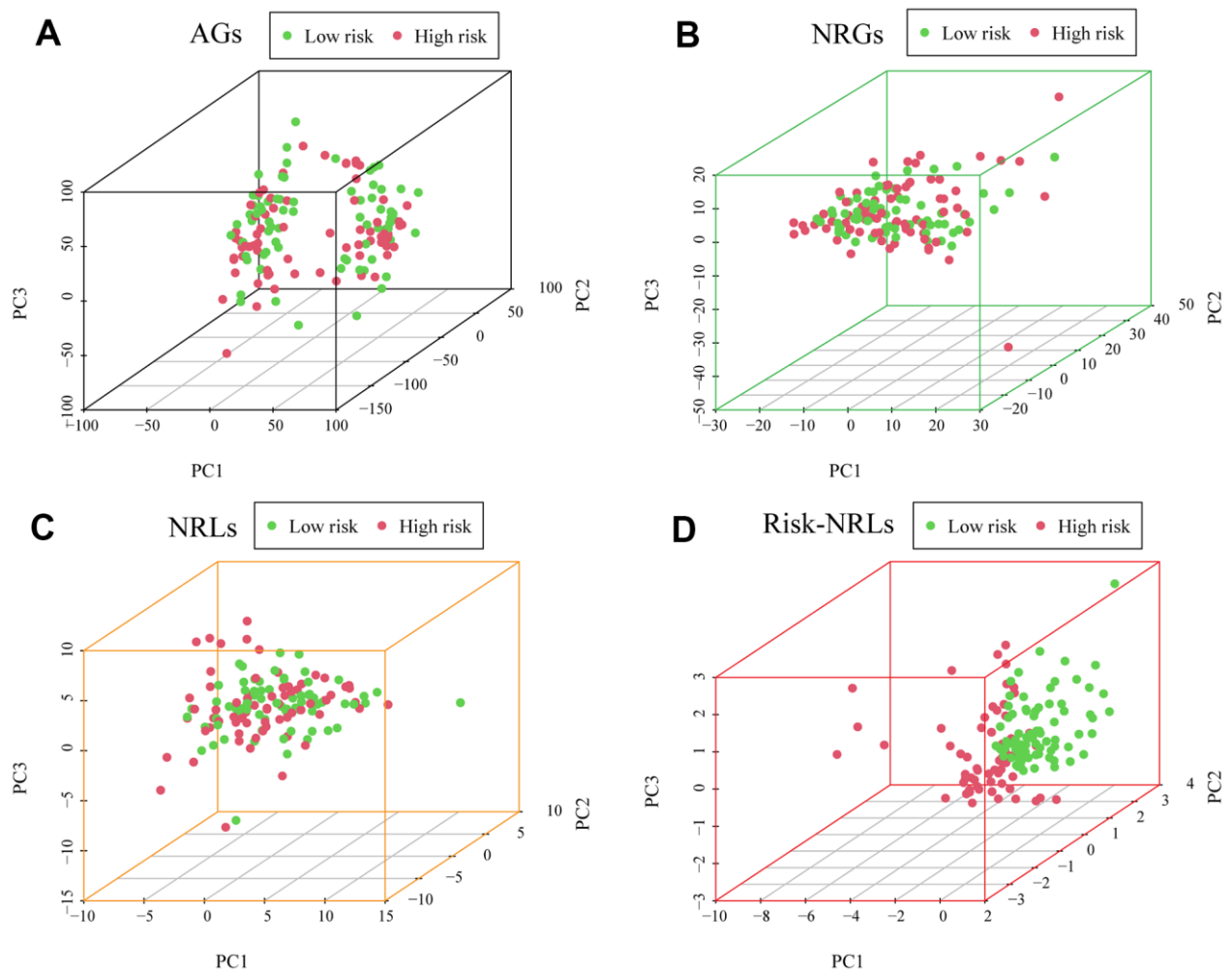
Supplementary Figure 2. Comparison of PCA models based on different gene sets. (**A**) PCA of all genes. (**B**) PCA of all necroptosis-related genes. (**C**) PCA of all co-expressed necroptosis lncRNAs. (**D**) PCA of six prognostic necroptosis-related lncRNAs.
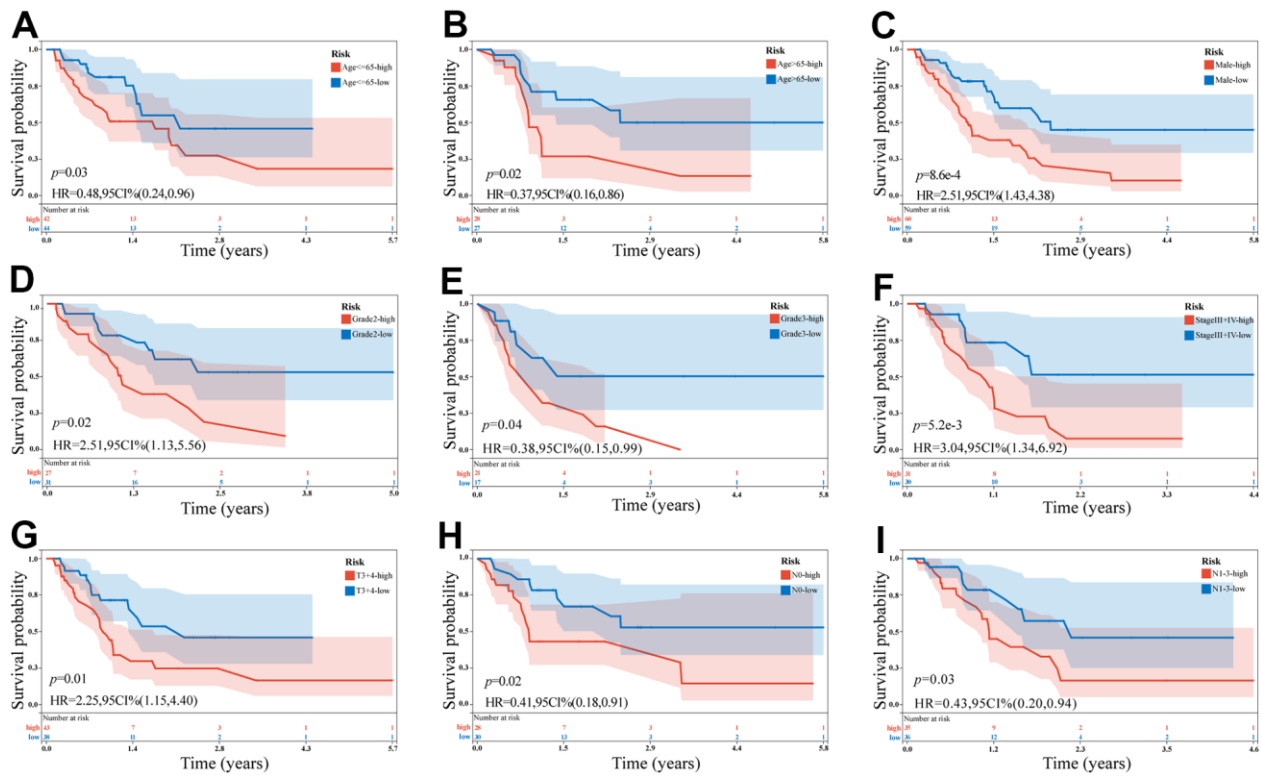
Supplementary Figure 3. Survival analysis of patients in high- and low-risk groups based on various clinicopathological features. Kaplan–Meier survival curves of (**A**, **B**) Age. (**C**, **D**) Male. (**D**, **E**) Grade. (**F**) Stage. (**G**) T. (**H**, **I**) N.
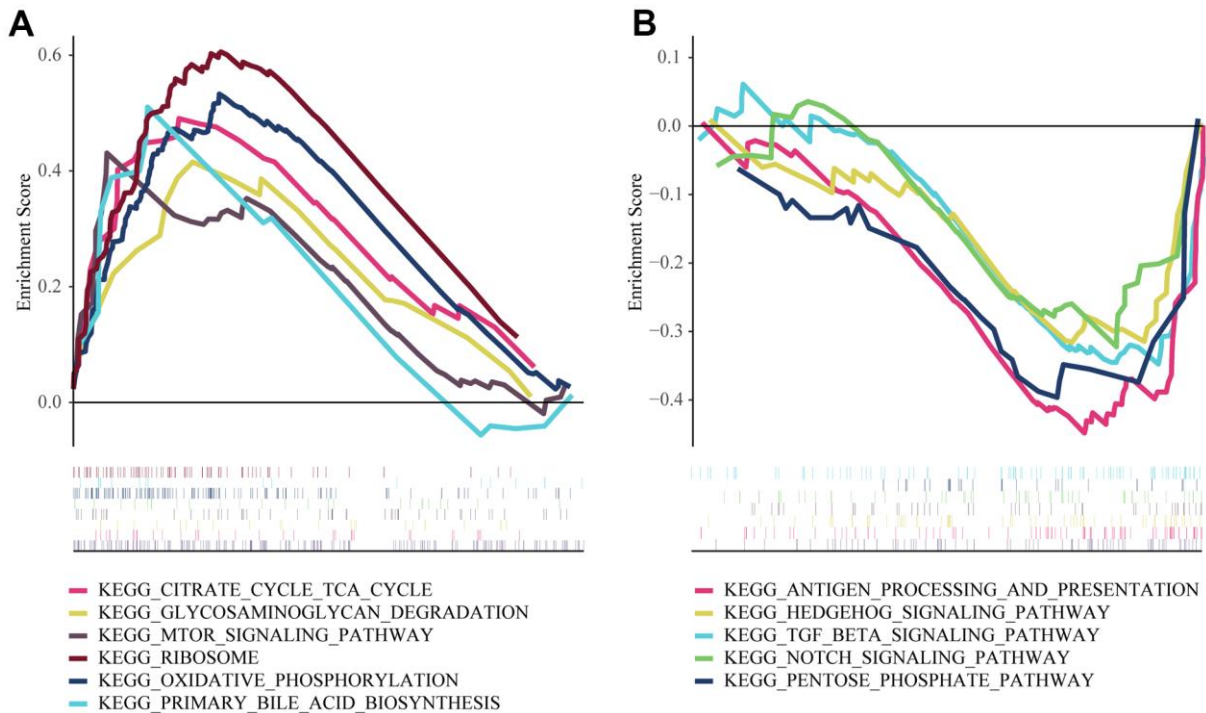
Supplementary Figure 4. GSEA enrichment analysis in ESCA patients from distinct risk groups. (**A**) GSEA enrichment analysis of ESCA patients in the high-risk group. (**B**) GSEA enrichment analysis of ESCA patients in the low-risk group.
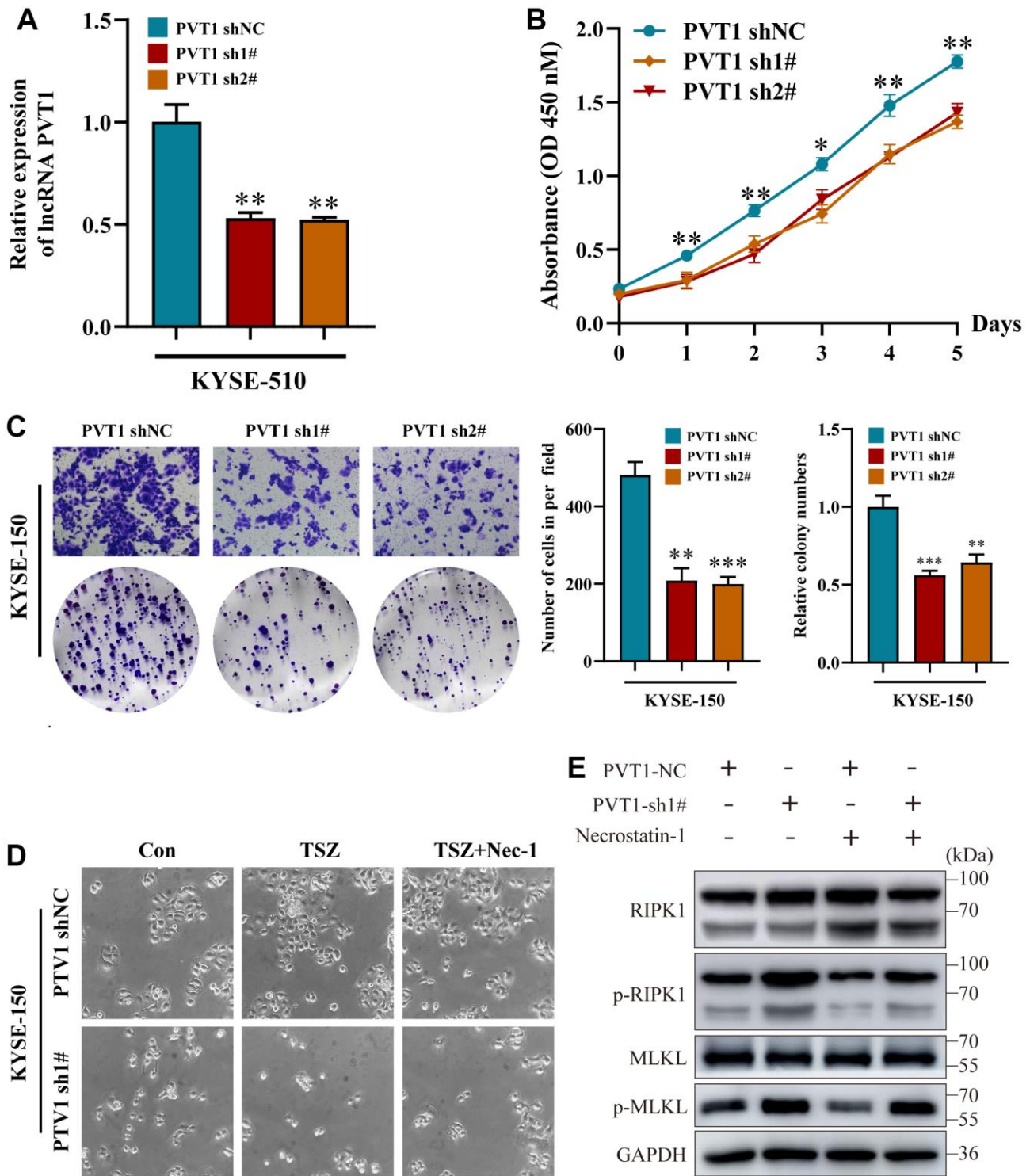
Supplementary Figure 5. PVT1 promoted KYSE-150 cell proliferation, migration, and inhibited necroptosis *in vitro*. (**A**) The transfection efficiency of PVT1 was downregulated using shRNAs. (**B**, **C**) Knockdown of PVT1 inhibited KYSE-150 cell proliferation and colony formation ability. (**D**) Both control and KYSE-150 PVT1-sh cells were treated with Nec-1 (50 μM) for 4 h and then treated with TSZ. After 24 h of drug treatment, the morphological changes of treated cells were imaged under a phase-contrast microscope. (**E**) Western Blot was performed to detect RIP1, p-RIP1, MLKL, and p-MLKL protein levels. Data are presented as mean ± SD (*p < 0.05; **p < 0.01; ***p < 0.001).

Supplementary Tables

Please browse Full Text version to see the data of Supplementary Tables 1, 4, 5.

Supplementary Table 1. A total of 159 necroptosis-related genes from KEGG.

Supplementary Table 2. The clinicopathological features of the ESCA patients.

Characteristic	Type	Training	Testing	Entire	*p*-value
Age	<=65	45(63.38%)	41(57.75%)	86(60.56%)	0.607
	>65	26(36.62%)	30(42.25%)	56(39.44%)	
Gender	FEMALE	12(16.90%)	10(14.08%)	22(15.49%)	0.817
	MALE	59(83.10%)	61(85.92%)	120(84.51%)	
Grade	G1	8(13.79%)	7(12.73%)	15(13.27%)	0.482
	G2	33(56.9%)	26(47.27%)	59(52.21%)	
	G3	17(29.31%)	22(40.00%)	39(34.51%)	
Stage	I	7(9.86%)	7(9.86%)	14(9.86%)	0.673
	II	30(42.25%)	36(50.70%)	66(46.48%)	
	III	27(38.03%)	24(33.80%)	51(35.92%)	
	IV	7(9.86%)	4(5.63%)	11(7.75%)	
T	T1	10(14.49%)	10(14.08%)	20(14.29%)	0.744
	T2	16(23.19%)	22(30.99%)	38(27.14%)	
	T3	40(57.97%)	37(52.11%)	77(55.00%)	
	T4	3(4.35%)	2(2.82%)	5(3.57%)	
M	M0	55(87.3%)	62(93.94%)	117(90.70%)	0.320
	M1	8(12.7%)	4(6.06%)	12(9.30%)	
N	N0	29(47.54%)	30(42.86%)	59(45.04%)	0.075
	N1	27(44.26%)	32(45.71%)	59(45.04%)	
	N2	3(4.92%)	5(7.14%)	8(6.11%)	
	N3	2(3.28%)	3(4.29%)	5(3.82%)	
Race	ASIAN	18(28.12%)	16(26.67%)	34(27.42%)	0.556
	WHITE	45(70.31%)	41(68.33%)	86(69.35%)	
	BLACK OR AFRICAN AMERICAN	1(1.56%)	3(5.00%)	4(3.23%)	
BMI	≤25	41(57.75%)	41(57.75%)	82(57.75%)	0.963
	>25	30(42.25%)	30(42.25%)	60(42.25%)	
New_events	Distant Metastasis	17(56.67%)	12(40%)	29(48.33%)	0.422
	Locoregional Recurrence	12(40.00%)	17(56.67%)	29(48.33%)	
	New Primary Tumor	1(3.33%)	1(3.33%)	2(3.33%)	
Radiotherapy	Local Recurrence	1(5.26%)	1(5.26%)	2(5.26%)	0.801
	Primary Tumor Field	8(42.11%)	10(52.63%)	18(47.37%)	
	Regional site	10(52.63%)	8(42.11%)	18(47.37%)	
Chemotherapy	NO	6(23.08%)	5(27.78%)	11(25.00%)	0.992
	YES	20(76.92%)	13(72.22%)	33(75.00%)	
Reflux_history	NO	33(61.11%)	38(62.3%)	71(61.74%)	0.438
	YES	21(38.89%)	23(37.7%)	44(38.26%)	

Supplementary Table 3. Primers and shRNA sequences used in this study.

Primers	
PVT1	**F:** 5'- TCAAGATGGCTGTGCCTGTC -3'
	R: 5'- TTCCACCAGCGTTATTCCCC -3'
GAPDH	**F:** 5'-GAACGGGAAGCTTGTCATCAA-3'
	R: 5'-ATCGCCCCACTTGATTTTGG-3'
shRNA	
shPVT1-1#	**F:**CCGGCCTGTTACACCTGGGATTTAGCTCGAGCT AAATCCCAGGTGTAACAGGTTTTTG
	R:AATTCAAAAACCTGTTACACCTGGGATTTAGCT CGAGCTAAATCCCAGGTGTAACAGG
shPVT1-2#	**F:**CCGGCCGGCGCTCAGCTGGGCTTGACTCGAGTC AAGCCCAGCTGAGCGCCGGTTTTTG
	R:AATTCAAAAACCGGCGCTCAGCTGGGCTTGACT CGAGTCAAGCCCAGCTGAGCGCCGG

Supplementary Table 4. Differential expression of necroptosis-related genes.

Supplementary Table 5. Differential expression of necroptosis-related lncRNAs.

Supplementary Table 6. Evaluation of 6-NRL signature based on time-dependent ROC and C-index.

Models	1 years	3 years	5 years	*p-value*	C-index[95%(CI)]	HR[95%(low, high)]	*p-value*	PMID
NRLs signature	0.784	0.827	0.764	<0.001	0.759[0.721, 0.797]	1.322(1.158-1.510)	<0.001	-
Song-JH signature	0.593	0.729	0.683	0.015	0.615[0.584, 0.646]	2.212(1.437-3.404)	<0.001	34291083
Ye-JC signature	0.611	0.704	0.709	0.006	0.599[0.569, 0.629]	2.251(1.353-3.747)	0.002	34764976
Zhao-MN signature	0.561	0.701	0.736	0.030	0.574[0.545, 0.603]	1.909(1.018-3.581)	0.044	35371305
Yao-JN signature	0.591	0.700	0.659	0.022	0.584[0.555, 0.613]	2.018(1.201-3.390)	0.008	34926275
Hu-ZN signature	0.573	0.700	0.780	0.028	0.552[0.524, 0.580]	1.910(0.818-4.460)	0.135	34840568
Yi-LL signature	0.747	0.688	0.627	0.002	0.659[0.626, 0.692]	1.651(1.298-2.101)	<0.001	32810627
Zhao-FC signature	0.610	0.688	0.666	0.286	0.573[0.544, 0.602]	2.430(0.750-7.872)	0.139	35309940
Wang-L signature	0.588	0.678	0.740	0.023	0.624[0.593, 0.655]	1.640(1.253-2.146)	<0.001	34257547
Zhao-FC signature	0.555	0.676	0.691	0.009	0.542[0.515, 0.569]	2.238(0.986-5.077)	0.054	35646892
Xiong-K signature	0.645	0.670	0.611	0.011	0.611[0.580, 0.642]	2.632(1.533-4.517)	<0.001	35497331
Zhuang-WT signature	0.652	0.669	0.579	0.003	0.619[0.588, 0.650]	1.924(1.058-3.500)	0.032	34976055
Liu-W signature	0.584	0.663	0.688	0.046	0.546[0.519, 0.573]	2.534(0.912-7.039)	0.075	36180848
Shi-XB signature	0.603	0.661	0.574	0.133	0.604[0.574, 0.634]	1.386(1.130-1.700)	0.002	35121801
Lian-L signature	0.619	0.644	0.637	0.020	0.602[0.572, 0.632]	1.973(1.305-2.982)	0.001	35557566
Zhang-CQ signature	0.583	0.636	0.658	0.029	0.577[0.548, 0.606]	1.952(1.009-3.774)	0.047	32883946
He-WW signature	0.650	0.634	0.640	0.254	0.599[0.569, 0.629]	2.367(1.389-4.036)	0.002	31423201
Xie-JH signature	0.528	0.628	0.741	0.241	0.531[0.504, 0.558]	1.512(1.123-2.036)	0.006	35282133
Xiao-WY signature	0.522	0.625	0.666	0.141	0.545[0.518, 0.572]	2.618(1.104-6.206)	0.029	35789548
Lan-T signature	0.583	0.615	0.694	0.444	0.565[0.537, 0.593]	2.456(1.180-5.112)	0.016	31966072
Chen-FN signature	0.558	0.613	0.703	0.020	0.566[0.538, 0.594]	1.939(1.247-3.013)	0.003	35611939
Zheng-ZJ signature	0.526	0.611	0.467	0.193	0.552[0.524, 0.580]	1.456(1.115-1.902)	0.006	35432441
Song-KW signature	0.566	0.606	0.730	0.048	0.560[0.532, 0.588]	2.038(1.172-3.544)	0.012	36072903
Zhang-CQ signature	0.581	0.599	0.602	0.203	0.558[0.530, 0.586]	2.753(0.776-9.763)	0.117	32898328
Sun-K signature	0.559	0.599	0.534	0.632	0.555[0.527, 0.583]	2.407(0.874-6.632)	0.089	35840882
He-ZK signature	0.598	0.594	0.693	0.121	0.596[0.566, 0.626]	2.523(1.126-5.650)	0.025	35574385
Cui-HY signature	0.531	0.593	0.562	0.218	0.524[0.498, 0.550]	2.801(0.353-22.198)	0.329	34336650
Zhao-FC signature	0.684	0.592	0.609	0.160	0.616[0.585, 0.647]	2.486(1.469-4.205)	<0.001	35912250
Liu-Y signature	0.608	0.592	0.522	0.120	0.596[0.566, 0.626]	2.499(1.449-4.310)	<0.001	32133283
Zhang-JF signature	0.606	0.589	0.535	0.223	0.587[0.558, 0.616]	1.947(1.398-2.711)	<0.001	35578166
Wu-D signature	0.682	0.583	0.579	0.113	0.604[0.574, 0.634]	2.242(1.100-4.567)	0.026	34170806
Peng-L signature	0.524	0.577	0.619	0.892	0.510[0.485, 0.536]	2.605(0.436-15.564)	0.294	31815134
Feng signature	0.608	0.568	0.598	0.630	0.577[0.548, 0.606]	1.506(1.199-1.892)	<0.001	34404882
Zhao-MN signature	0.573	0.568	0.571	0.313	0.574[0.545, 0.603]	2.435(0.826-7.174)	0.106	35899307
Xu-T signature	0.504	0.561	0.746	0.447	0.501[0.476, 0.526]	2.359(0.524-10.628)	0.264	35116551
Zhu-T signature	0.524	0.558	0.480	0.336	0.542[0.515, 0.569]	2.468(0.839-7.263)	0.101	33748133
Pang-JJ signature	0.671	0.554	0.730	0.049	0.629[0.598, 0.660]	2.602(1.168-5.800)	0.002	34659345
Du-HL signature	0.540	0.552	0.529	0.213	0.542[0.515, 0.569]	2.264(0.713-7.192)	0.166	33708944
Pu-Y signature	0.577	0.548	0.497	0.221	0.573[0.544, 0.602]	2.200(0.673-7.190)	0.192	35284129
Chen-YH signature	0.586	0.545	0.535	0.238	0.550[0.523, 0.578]	2.199(1.024-4.721)	0.043	33960364
Zhang-HP signature	0.622	0.537	0.561	0.485	0.579[0.550, 0.608]	1.782(1.111-2.859)	0.017	34234806
Chen-FF signature	0.511	0.528	0.492	0.639	0.504[0.479, 0.529]	2.442(0.362-16.458)	0.359	35928921
Meng-J signature	0.620	0.524	0.469	0.179	0.594[0.564, 0.624]	2.782(1.202-6.440)	0.017	29160958
Zhang-WG signature	0.473	0.523	0.691	0.731	0.468[0.445, 0.491]	2.514(0.378-16.734)	0.341	36071753
Tan-LL signature	0.546	0.489	0.465	0.494	0.560[0.532, 0.588]	2.135(0.935-4.876)	0.072	34814273
Lu-T signature	0.523	0.464	0.348	0.514	0.595[0.565, 0.625]	2.193(0.591-8.144)	0.241	33981829
Gao-JY signature	0.534	0.455	0.360	0.937	0.536[0.509, 0.563]	2.349(0.243-22.697)	0.460	33718151
Zhang-CQ signature	0.614	0.451	0.424	0.304	0.576[0.547, 0.605]	2.335(0.947-5.754)	0.065	33392181
Zhang-CQ signature	0.544	0.408	0.302	0.695	0.547[0.520, 0.574]	3.217(0.038-269.472)	0.605	35224157

Supplementary Table 7. Top 20 categories with their representative enriched terms (one per category).

GO	Category	Description	Count	%	Log10(P)	Log10(q)
hsa04217	KEGG Pathway	Necroptosis	27	100	-62.53	-58.18
hsa05164	KEGG Pathway	Influenza A	12	44.44	-19.92	-15.88
WP4630	WikiPathways	Measles virus infection	8	29.63	-12.55	-8.89
R-HSA-9645723	Reactome Gene Sets	Diseases of programmed cell death	7	25.93	-11.37	-7.98
R-HSA-5218859	Reactome Gene Sets	Regulated Necrosis	6	22.22	-10.86	-7.52
hsa04621	KEGG Pathway	NOD-like receptor signaling pathway	7	25.93	-9.62	-6.61
GO:0009615	GO Biological Processes	response to virus	8	29.63	-9.13	-6.25
GO:0070663	GO Biological Processes	regulation of leukocyte proliferation	7	25.93	-8.51	-5.76
GO:0000302	GO Biological Processes	response to reactive oxygen species	6	22.22	-8.08	-5.41
GO:0043124	GO Biological Processes	negative regulation of I-kappaB kinase/NF-kappaB signaling	4	14.81	-6.91	-4.49
R-HSA-1280215	Reactome Gene Sets	Cytokine Signaling in Immune system	8	29.63	-6.78	-4.38
GO:0002260	GO Biological Processes	lymphocyte homeostasis	4	14.81	-6.48	-4.16
GO:0080135	GO Biological Processes	regulation of cellular response to stress	7	25.93	-5.58	-3.52
GO:0038034	GO Biological Processes	signal transduction in absence of ligand	3	11.11	-5.47	-3.44
WP5083	WikiPathways	Neuroinflammation and glutamatergic signaling	4	14.81	-5.14	-3.17
GO:0001933	GO Biological Processes	negative regulation of protein phosphorylation	5	18.52	-4.93	-2.99
GO:0009612	GO Biological Processes	response to mechanical stimulus	4	14.81	-4.41	-2.54
WP2037	WikiPathways	Prolactin signaling pathway	3	11.11	-4.37	-2.51
GO:1901216	GO Biological Processes	positive regulation of neuron death	3	11.11	-4.12	-2.29
GO:0071496	GO Biological Processes	cellular response to external stimulus	4	14.81	-3.76	-1.97